Stem Cell Reports
Article

OPEN ACCESS

Sox10 Regulates Plasticity of Epithelial Progenitors toward Secretory Units of Exocrine Glands

Harleen K. Athwal,[1,2,4] George Murphy III,[1,2,4] Ellis Tibbs,[3,4] Ashley Cornett,[1,2] Emily Hill,[1,2] Kenji Yeoh,[1,2] Elsa Berenstein,[3] Matthew P. Hoffman,[3] and Isabelle M.A. Lombaert[1,2,3,*]

[1]University of Michigan, Biointerfaces Institute, 2800 Plymouth Road, Ann Arbor, MI, USA
[2]University of Michigan, School of Dentistry, Department of Biologic and Materials Sciences, 2800 Plymouth Road, Ann Arbor, MI 48109, USA
[3]National Institutes of Dental and Craniofacial Research, National Institutes of Health, 30 Convent Drive, Bethesda, MD 20892, USA
[4]Co-first author
*Correspondence: lombaert@umich.edu
https://doi.org/10.1016/j.stemcr.2019.01.002

SUMMARY

Understanding how epithelial progenitors within exocrine glands establish specific cell lineages and form complex functional secretory units is vital for organ regeneration. Here we identify the transcription factor *Sox10* as essential for both the maintenance and differentiation of epithelial KIT$^+$FGFR2b$^+$ progenitors into secretory units, containing acinar, myoepithelial, and intercalated duct cells. The KIT/FGFR2b-*Sox10* axis marks the earliest multi-potent and tissue-specific progenitors of exocrine glands. Genetic deletion of epithelial *Sox10* leads to loss of secretory units, which reduces organ size and function, but the ductal tree is retained. Intriguingly, the remaining duct progenitors do not compensate for loss of *Sox10* and lack plasticity to properly form secretory units. However, overexpression of *Sox10* in these ductal progenitors enhances their plasticity toward KIT$^+$ progenitors and induces differentiation into secretory units. Therefore, *Sox10* controls plasticity and multi-potency of epithelial KIT$^+$ cells in secretory organs, such as mammary, lacrimal, and salivary glands.

INTRODUCTION

Cellular plasticity is an important feature within adult organs facilitating rapid adaptation of progenitors to injury or environmental changes. Previously, it was thought that progenitors within organs would respond to injury in a uni-directional cell lineage manner. A series of differentiation steps producing multiple cell intermediates, each with a more restricted lineage potential than the last, would eventually lead to specialized cells. Recent reports challenge this paradigm showing that cells can acquire characteristics of other cell types beyond their proposed lineage (Tata and Rajagopal, 2016) by converting into earlier cell types (de-differentiation), more distant phenotypes (trans-differentiation), or interchange between different progenitors (trans-determination). Each of these three cellular processes may occur in different settings and to various degrees (Donati and Watt, 2015). Interestingly, both cell-autonomous and non-cell-autonomous mechanisms are proposed to contribute to this plasticity. Environmental factors, such as cell-cell contact or ligand presentation, contribute to non-cell-autonomous induction. Whereas transcription factors (TFs) are part of the autonomous mechanism, playing a major role in regulating cell fate, stability, and conversion. However, very little is known about how plasticity is regulated, and how it varies among cell types and different conditions.

Exocrine glands, such as the mammary, lacrimal, and salivary glands, all share a similar secretory function that entails production and secretion of milk, tears, and saliva, respectively (Wang and Laurie, 2004). They all undergo branching morphogenesis to create a ductal tree structure distally ending in secretory units whereby fluid can be produced, modified, transported, and released from the gland. These secretory units include secretory acinar cells, associated intercalated ducts that connect larger ducts to the acini, and contractile myoepithelial cells surrounding the acini (Lombaert et al., 2017). As such, it was postulated that various signaling pathways and cellular mechanisms must overlap among these exocrine glands (Wang and Laurie, 2004). For example, the TF MIST1 was identified as a "scaling factor" to induce and maintain the secretory cell architecture of mature acinar cells in multiple exocrine tissues (Lo et al., 2017). However, which specific TFs control and direct epithelial progenitors to form the secretory units, and whether common TFs are involved in different organs are unknown.

TFs whose activity is necessary and sufficient to direct specific cell lineage commitment, and that can also respecify the fate of cells destined to become other lineages, are termed core master regulators (Chan and Kyba, 2013). Master regulators promote gene transcription to initiate or maintain the desired cell fate, and repress gene expression that oppose this decision; ultimately stabilizing cell fate decisions. Here we identify *Sox10* as a master regulator to maintain and direct KIT$^+$ progenitors into secretory units of exocrine glands. SOX proteins have previously been described as mediators of both stemness and cell differentiation (Abdelalim et al., 2014), and *Sox10* is well-known for its role in neural crest stem cell maintenance and their differentiation into oligodendrocytes and glia cells (Reiprich and Wegner, 2015). Surprisingly, more recent studies

reported SOX10 in epithelial cell types of exocrine mammary, lacrimal, and salivary glands (Chen et al., 2014; Dravis et al., 2015; Lombaert et al., 2013). Using salivary glands as our primary model system, we report that *Sox10* is an exocrine gland-specific core master regulator that is sufficient to induce plasticity and multi-potency of tissue-specific progenitors to form functional secretory units.

RESULTS

The KIT/FGFR2b-*Sox10* Axis Defines Initial Tissue-Specific Cells

To identify tissue-specific progenitors, we analyzed protein expression of known markers of adult and fetal salivary submandibular gland (SMG) progenitors. Adult SMG progenitors expressing CD117 (KIT, c-Kit) were previously shown to regenerate radiation-damaged mouse SMGs *in vivo* by differentiating into saliva-secreting acinar and saliva-transporting duct cells (Lombaert et al., 2008). However, their presence and function at SMG ontogenesis (embryonic day 11.5 [E11.5]) remained unclear. SMGs, such as the parotid (PAR) and sublingual (SLG) salivary glands, derive from an invagination and thickening of oral epithelium (Knosp et al., 2012). This thickened epithelium forms a single endbud, termed cap or tip cells in other exocrine glands, which clefts to generate multiple distal endbuds on a lengthening proximal duct. We found that KIT$^+$ cells are present at SMG initiation, as protein staining of enzymatically isolated epithelia from E11.5–E12 embryos showed membrane localization of KIT on the oral epithelial lining, initial single SMG endbud, and main duct (Figures 1A and S1A). By E13, however, KIT expression becomes restricted to endbuds only (Figure S1A) (Lombaert et al., 2013). These KIT$^+$ progenitors require FGFR2b signaling for cell survival, cell proliferation, and initiation of SOX10 expression to become uniquely distinct from the SOX2$^+$KIT$^-$ main ducts (Lombaert et al., 2013; Lombaert and Hoffman, 2010). Thus, as oral epithelial cells express KIT at gland initiation, we hypothesized that KIT/FGFR2b-regulated TFs specify the initial tissue-specific progenitors. We show that, during the initial oral budding, SOX10$^+$ cells are localized in the distal epithelia while proximal layers expressed SOX2$^+$ (Figures 1A–1C). Sporadically, a SOX2$^+$SOX10$^+$ cell was found at the border of both cell layers (Figure 1C, arrows), suggesting a potential transitioning cell. The oral epithelium is known to express *Sox2*, *ΔNp63*, *Fgfr2b*, and intracellular cytokeratins KRT14 (K14) and KRT5 (K5) (Jones and Klein, 2013; Rice et al., 2004). Protein analysis of KRT's in E11.5–E12 isolated epithelia revealed two distinct layers, in a similar manner to SOX2 and SOX10 expression. Proximal cells co-expressed K14, K5, and K19, while distal cells were enriched for K14$^+$ (Figures S1B and S1C). SOX2 expression overlapped with K14$^+$K5$^+$ proximal cells and SOX10 was co-expressed in K14$^+$ distal cells (Figure S1D); confirming the positioning of two distinct epithelial layers at SMG ontogenesis.

To investigate the role of FGFR2b signaling in specifying the tissue-specific distal epithelial progenitors, we analyzed the initiating glands of *Fgf10*$^{-/-}$ murine embryos, which lack the ligand for FGFR2b and die at birth due to severe abnormalities in multiple organs. E11.5 *Fgf10*$^{-/-}$ isolated SMG epithelia expressed SOX2 but failed to express SOX10, even though surrounding neuronal cells (CDH1/E-cadherin-negative) clearly expressed SOX10 (Figure S1E, arrow). As FGF10/FGFR2b signaling is the primary signal to initiate *Sox10*$^+$ cells, we isolated and cultured wild-type E12 epithelia for 2 h in basal medium +/− FGF10. Within this time frame, *Sox2* expression was downregulated and *Sox10* was upregulated (Figure S1F), suggesting that FGF10/FGFR2b signaling induces the switch from SOX2$^+$ into SOX10$^+$ cells.

To confirm that the KIT/FGFR2b-*Sox10* axis was important in other exocrine glands, we evaluated distal cells in lacrimal, PAR, SLG, and mammary glands (MMGs). The SLG was the only exception where SOX2 was expressed in distal KIT$^+$ cells. The other exocrine glands exclusively expressed KIT and SOX10 (Figure 1D), and all salivary glands shared a similar epithelial KRT-expressing cell population (Figure 1E).

Thus, we identified two distinct KIT$^+$ epithelial cell layers present at SMG initiation: proximal SOX2$^+$ oral epithelial cells and distal SOX10$^+$ cells that initiate in an *Fgf10*-dependent manner. Collectively, these data suggest that SOX10 defines the initial endbud cells of exocrine glands.

Glandular Tissues Originate from Oral Epithelial *Sox2* Cells

To elucidate the contribution of SOX2$^+$ oral epithelial and SOX10$^+$ cells to tissue formation, we used lineage tracing to visualize their progeny. *Sox2*-Cre mice crossed with *Rosa26-*^{flox}mTomato^{flox}-mGFP (mTmG) mice showed that the SMG is mGFP$^+$, demonstrating that SMGs are offspring of *Sox2* cells (Figure S2A). This is consistent with data that SOX2 is first expressed by pluripotent embryonic stem cells at E2.5–E3.5, and thus expected to give rise to all glands (Avilion et al., 2003). Next, tamoxifen-inducible *Sox2*-Cre mice allowed us to specifically track progeny of E9–E11 oral epithelial cells. Consistent with previous literature (Rothova et al., 2012; Tucker, 2007), we found that all (E13) epithelial cells, including SOX10$^+$ cells, arose from E9 to E11 *Sox2* oral epithelia (Figure 2A). The E9–E11 *Sox2* cells also contributed to epithelial cells in adult SMGs, as well as their inter-glandular ducts, which connect the organ to the oral cavity (Figure 2B, arrows). Inter-glandular ducts are comprised of two types of ducts that transport saliva outside the organ: excretory ducts (EDs) that connect with one main Wharton's duct (WD, SMG) or Bartholin's duct (BD, SLG).

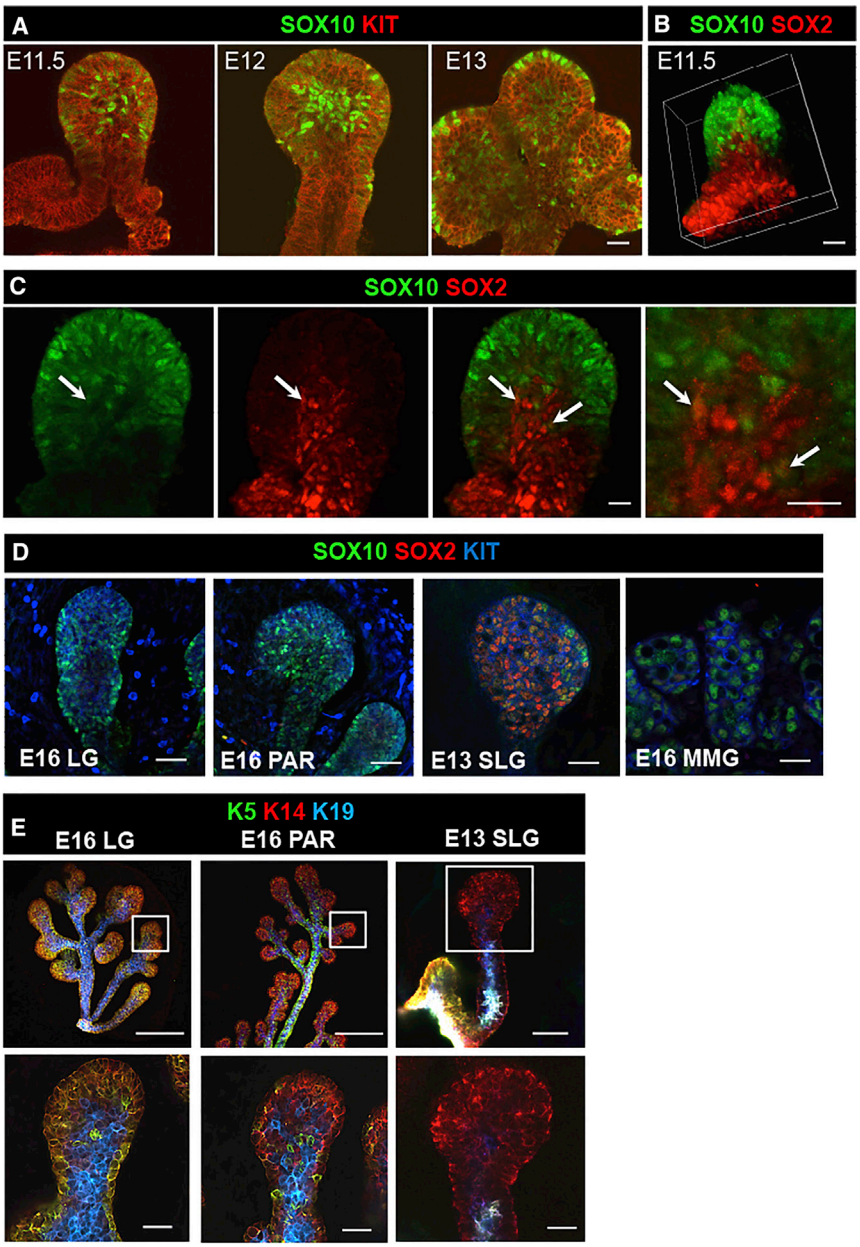

Figure 1. The KIT/FGFR2b-*Sox10* Axis Defines Initial Tissue-Specific Cells

(A) Confocal images of E11.5, E12, and E13 isolated SMG epithelia stained for SOX10 and KIT. Scale bars, 20 μm.

(B) E11.5 isolated epithelium stained for SOX10 and SOX2. Scale bars, 20 μm.

(C) SOX10 and SOX2 expression in E11.5 epithelium. Arrows outline SOX10$^+$SOX2$^+$. Scale bars, 20 μm.

(D and E) Confocal images of E16 LG, E16 PAR, E13 SLG, and E16 MMG. Tissue was stained for SOX10, SOX2, and KIT, or K14, K5, and K19. Scale bars, 100 μm (D) and 20 μm (E).

We hypothesized that SOX2$^+$ oral epithelial cells would not contribute to organ formation after initiation of the SOX10$^+$ cells in the distal endbud. Indeed, induction of *Sox2*-Cre at E12–E13, after SMG initiation, supported our hypothesis, as *Sox2* cells no longer contributed to SMG development (Figures 2C and S2B). In addition, the intraglandular ducts, such as striated ducts (SD), were mGFP-negative. However, various portions of the larger interglandular ducts as well as cells in SLGs did derive from E12 to E13 *Sox2*$^+$ cells (Figure S2B, arrows). This result supports our previous data that basal cells in the main duct of developing SMGs remain SOX2$^+$ (Lombaert et al., 2011), and that SOX2 is present in distal cells of SLGs (Figure 1D). These data thus suggest that all salivary glandular tissue is derived from the *Sox2*$^+$ oral epithelium at E9–E11, but thereafter more restricted tissue-specific progenitor cell contributes to organ development.

The Initial *Sox10*$^+$ Cells Are Multi-potent Progenitors of Secretory Units

We next investigated the contribution of *Sox10* epithelial cells during development. Lineage tracing with a constitutive *Sox10*-Cre mouse confirmed the unique location of SOX10$^+$ cells in distal epithelial endbuds (E12–E13)

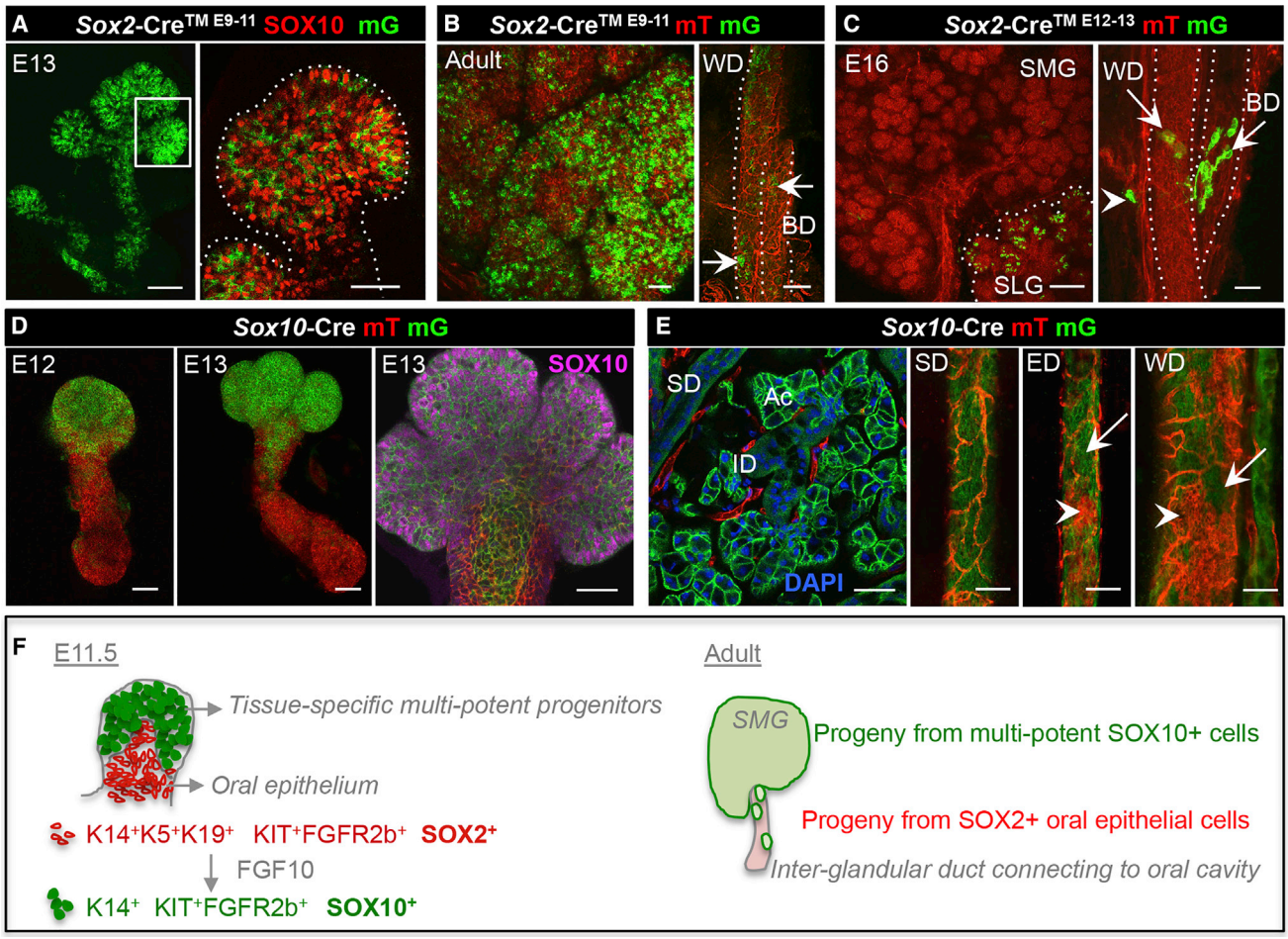

Figure 2. Initial Tissue-Specific SOX10$^+$ Cells Are Multi-potent Progenitors

Sox2-Cre^{TM} or Sox10-Cre mice were crossed with Rosa26-mTmG mice for lineage tracing. mGFP$^+$ (mG) cells are lineage-derived cells, mTomato (mT) cells are not.

(A and B) E9–E11 induced lineage tracing seen in isolated E13 epithelia (A) or adult SMG (B). E13 epithelium was co-stained with SOX10. Scale bars: (A, left and B, left) 100 μm; (A, right and B, right) 20 μm. WD, SMG Wharton's duct; BD, SLG Bartholin's duct. Arrows outline mG$^+$ cells.

(C) Confocal images of E16 SMG with WD, and SLG with BD. Tissue was lineage traced from E12–13. Scale bar, 100 μm.

(D) Isolated epithelia were analyzed by confocal microscopy at E12 and E13. E13 epithelium was co-stained for SOX10. Scale bars, 100 μm (left and middle) and 20 μm (right).

(E) Confocal imaging of adult SMG intra-glandular striated ducts (SD), inter-glandular excretory ducts (EDs) and WDs. Arrowheads and arrows represent mT and mG epithelial cells, respectively. Acinar cell (Ac), intercalated duct (ID). Scale bars, 20 μm (left) and 200 μm (centers and right).

(F) Graphical cartoon depicting the presence of two epithelial cell types after E11.5 SMG initiation: SOX2$^+$ oral epithelial cells co-expressing K14, K5, and K19, and distal SOX10$^+$ tissue-specific SMG cells solely co-expressing K14. Both cell types express KIT and FGFR2b, but contribute differentially to adult glands. Once tissue-specific cells are formed, oral epithelial cells only contribute to parts of the inter-glandular ducts connecting the secretory organ with the oral cavity. Instead, *Sox10* cells form all epithelial cells in the adult SMG, as well cells parts in inter-glandular ducts.

(Figure 2D). Up to 99.9% ± 0.1% and 98.3% ± 0.6% of all myoepithelial and acinar cells were *Sox10*-derived (Figure S2C), respectively, as quantified by co-expression with mGFP in adult *Sox10*-Cre mice. On the other hand, cells of the inter-glandular ducts (EDs and WDs) were not entirely *Sox10* derived, and these non-*Sox10*-derived offspring became more prominent in the WD (Figure 2E, arrowheads). Interestingly, distal parts of these inter-glandular ducts, were *Sox10* derived (Figure 2E, arrows), suggesting that inter-glandular ducts may be derived from both

oral epithelium and SOX10$^+$ cells. This pattern was apparent during development (E14) where distal parts of the duct remain *Sox10*$^+$ (Figure S2D). However, adult intra-glandular epithelia were exclusively mGFP$^+$ (Figure 2E), which could be observed by co-staining with an epithelial marker K8, myoepithelial marker alpha-smooth muscle actin (ACTA2), and acinar cell-specific water channel aquaporin5 (AQP5) (Figure S2D). In fact, the parenchyma and inter-glandular ducts of adult lacrimal and PAR glands were also entirely *Sox10* derived (Figure S2E), while the SLG epithelial cells were both *Sox2* and *Sox10* derived. When *Sox10*-rtTA;*Tet*-Cre mice were induced at E9–12, the analysis confirmed the exclusive contribution of the initial *Sox10* cells to adult SMG organ formation. The acinar (84.3% ± 1.2%), myoepithelial (85.4% ± 4.1%) and ductal (97.3% ± 4.5%) cells co-expressed mGFP, suggesting that initial *Sox10* cells form the entire SMG epithelium (Figure S2F). Taken together, these data identify *Sox10* as an early marker of multi-potent tissue-specific epithelial progenitors of exocrine glands (Figure 2F).

Loss in *Sox10* Reduces Exocrine Gland Development

We next identified mechanisms through which *Sox10* regulates cellular processes. There was ~64% overlapping protein expression of SOX10 with CCND1 or KI67 in distal E13 KIT$^+$ progenitors, suggesting that *Sox10* could regulate cell proliferation (Figures 3A and S3A). At E16, secretory cell differentiation begins and KIT$^+$ progenitors could lose potency by either downregulating *Sox10* or becoming quiescent. Quantification of SOX10 and/or CCND1 in E16 KIT$^+$ progenitors indicated that SOX10 remained highly expressed in proliferating cells.

To determine the function of *Sox10* during organ formation, we analyzed glands from *Sox10*$^{flox/flox}$ mice crossed with epithelial-specific *Krt14*-Cre (referred as *Sox10*$^{fl/fl}$) and/or *Rosa26*-mTmG mice (Figure S3B). Fetal (E13, E14, and E16) SMGs were evaluated for mGFP and loss of SOX10 (Figures 3B–3D and S3C). Non-epithelial cells remained mTomato$^+$, and, as expected, SOX10 was only detected in TUBB3$^+$ neuronal cells (Figure 3C). These data suggested that the *Krt14*-Cre;*Sox10*$^{fl/fl}$ system specifically and efficiently targets epithelial *Sox10*.

We next measured the impact of *Sox10* loss on branching morphogenesis in SMG (Figures 3D and 3E). There was a significant reduction in endbud number at both E13.5 and E14 (40%), and 50% at E16 (Figure S3D). Notably, endbud counts becomes less accurate at E16; however, the remaining ductal tree structure became visible with reduced endbuds, as noticed in higher magnifications (Figure 3D). There was a 50% reduction in mGFP intensity in E16 *Krt14*-Cre;*Sox10*$^{fl/f}$;*mTmG* glands (Figure 3E), which reflected the reduction in epithelial size. This morphology was similar in post-natal SMGs (Figure S3E). Similar impacts on organ formation of lacrimal, PAR, and SLG glands were observed, where distal branching and/or endbud numbers were significantly decreased (Figures S3F and S3G). These data highlight that *Sox10* is necessary for proper organ formation induced by KIT$^+$ endbud progenitors.

Sox10 Is Essential for KIT$^+$ Progenitor Maintenance and Differentiation into Secretory Units

To identify how *Sox10* influences progenitors, we performed protein and transcriptome profiling of known markers that define SMG progenitors in both control and *Sox10*$^{fl/fl}$ E16 SMGs. Proliferating KIT$^+$ progenitors are present in distal endbuds, but the remaining distal cells in *Sox10*$^{fl/fl}$ SMGs did not show KIT and had reduced CCND1 (Figures 4A and 4B). While cell apoptosis occurs in developing organs as part of size expansion and differentiation (Teshima et al., 2016), no differences in cleaved caspase-3 were observed in epithelia or surrounding cells of *Sox10*$^{fl/fl}$ SMGs (Figure S4A). This suggests that *Sox10* directly affects KIT$^+$ cell maintenance via proliferation. Alternatively, K14 and K5 expression, which mark basal and supra-basal duct cells that comprise a subpopulation of KIT$^+$ cells (Lombaert et al., 2013), were unaffected by *Sox10* loss, nor were their ductal K19$^+$ and/or K7$^+$ offspring or the *Wnt*/*Egfr*-related signaling pathway (Figures 4A and 4B). The expression of the KIT/FGFR2b signaling pathway (Lombaert et al., 2013), including receptors *Kit* and *Fgfr1b* along with downstream targets *Etv5*, *Sox10*, and heparan sulfate (Figure 4B), were reduced in *Sox10*$^{fl/fl}$ SMGs. In parallel, surface markers integrin alpha 6 (*Itga6*, *CD49f*), beta 1 (*Itgb1*, *CD29*), and CD24, which can enrich for adult SMG progenitors, remained unaltered, as did TF *Sox9* (Figure S4B). SOX9 is expressed by distal and proximal cells in salivary and lacrimal glands, and is required for SOX10 expression (Chatzeli et al., 2017; Chen et al., 2014). In wild-type SMGs, *Sox9* is regulated by KIT/FGFR2b signaling, as stimulation of isolated E13 epithelia with FGF10 (F10) and/or KIT ligand (K) rapidly upregulated *Sox9* in 3 h (Figure S4C), confirming the Chatzeli et al. study in which *Sox9* was absent in the SLG/SMG of *Fgf10*$^{-/-}$ mice. Nonetheless, SOX9 protein expression remained present in basal epithelial and surrounding cell types in *Sox10*$^{fl/fl}$ SMGs (Figure S4D), suggesting that loss of *Sox10* and the subsequent reduction in KIT/FGFR2b signaling did not directly impact *Sox9*. Lastly, progenitors that form later in development were also evaluated. One progenitor population expressing the TF *Ascl3*, is detectable at E16 and is bipotent as it contributes to a subpopulation of adult SMG ductal and acinar cells (Bullard et al., 2008). To our surprise, *Ascl3* expression was upregulated in *Sox10*$^{fl/fl}$ SMGs (Figure S4B), which may be due to either decreased distal to proximal cell ratio or direct

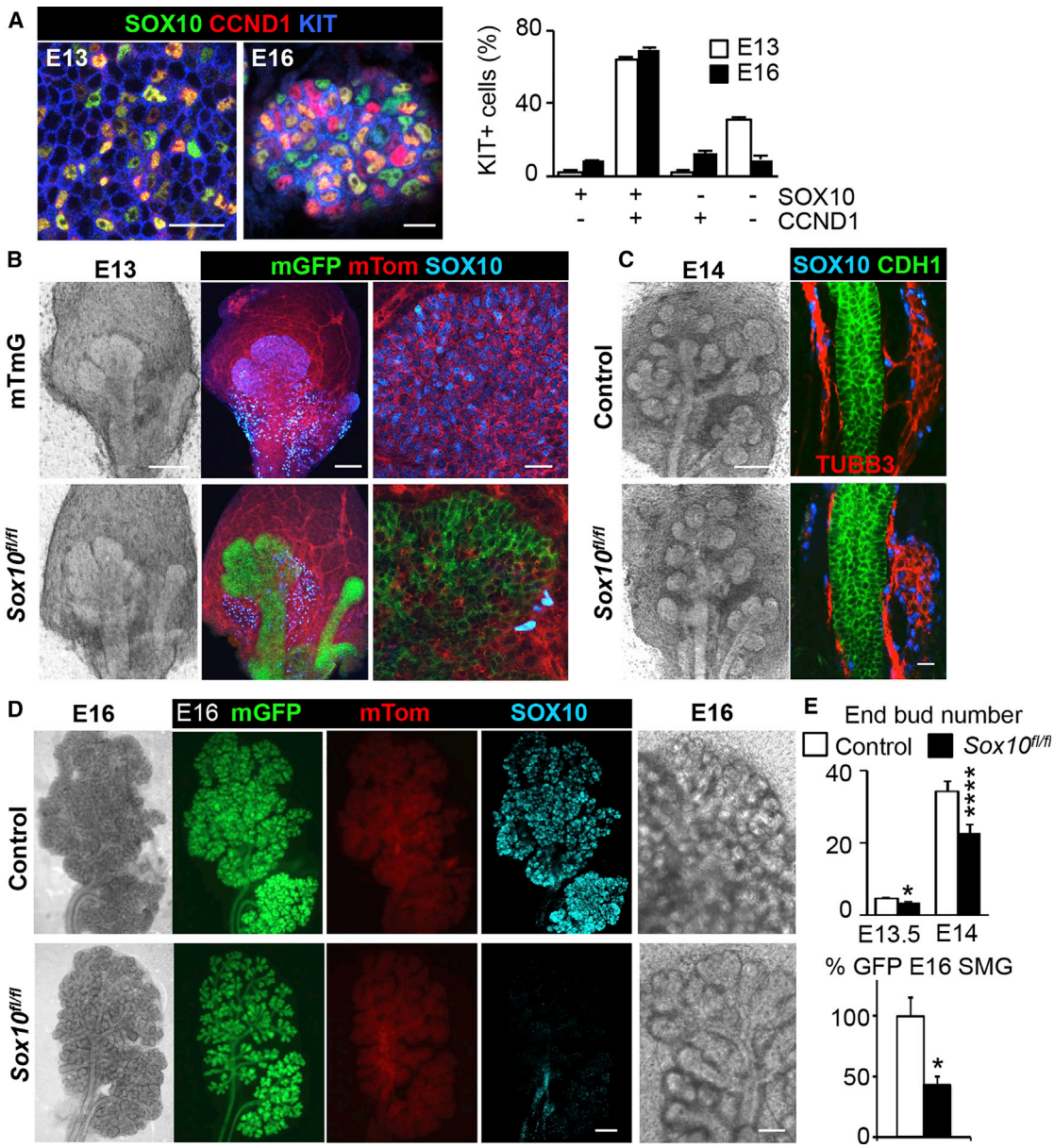

Figure 3. Loss in *Sox10* Negatively Impacts Exocrine Gland Formation

(A) Confocal pictures of KIT, SOX10, and CCND1 co-staining in E13 and E16 SMG endbuds. Scale bars, 20 μm. Graph represents KIT^{+} subpopulations counted on multiple sections through endbuds at each time point. N > 3, Mean ± SEM.

(B and C) Bright-field and confocal pictures of E13 (B) and E14 (C) control (*Krt14*-Cre;*Rosa26*-mTmG;*Sox10*$^{flox/+}$ or *Rosa26*-mTmG or *Sox10*$^{flox/flox}$ mice) and *Sox10*$^{fl/fl}$ (*Krt14*-Cre;*Rosa26*-mTmG;*Sox10*$^{flox/flox}$) SMGs. SMGs were labeled for SOX10, TUBB3, and CDH1. Scale bars, 100 and 20 μm.

(D) Bright-field and fluorescent images of E16 control and *Sox10*$^{fl/fl}$ SMGs. SMGs were stained for SOX10. Scale bars, 500 and 250 μm.

(E) Quantification of endbud number in E13.5 and E14 SMGs from control and *Sox10*$^{fl/fl}$ mice. Mean ± SEM, N > 3, unpaired t test. *p < 0.05, ****p < 0.0001. Control E13 (4.5 ± 0.4) versus *Sox10*$^{fl/fl}$ (3.4 ± 0.2), control E14 (34.2 ± 2.8) versus *Sox10*$^{fl/fl}$ (22.7 ± 2.4). Graph depicting GFP expression in E16 control and *Sox10*$^{fl/fl}$ SMGs. Data are normalized to control, mean ± SEM, N > 3, unpaired t test. *p < 0.05. Control (100.0% ± 15.8%) versus *Sox10*$^{fl/fl}$ (43.1 ± 7.2%).

compensation in response to loss of *Sox10*. Overall, these data illustrate that *Sox10* is essential for the maintenance and proliferation of KIT^{+} progenitors.

The observation that E16 *Sox10*$^{fl/fl}$ SMGs had aberrant morphology led us to hypothesize that *Sox10* affects differentiation. At E16, the differentiation of proacinar,

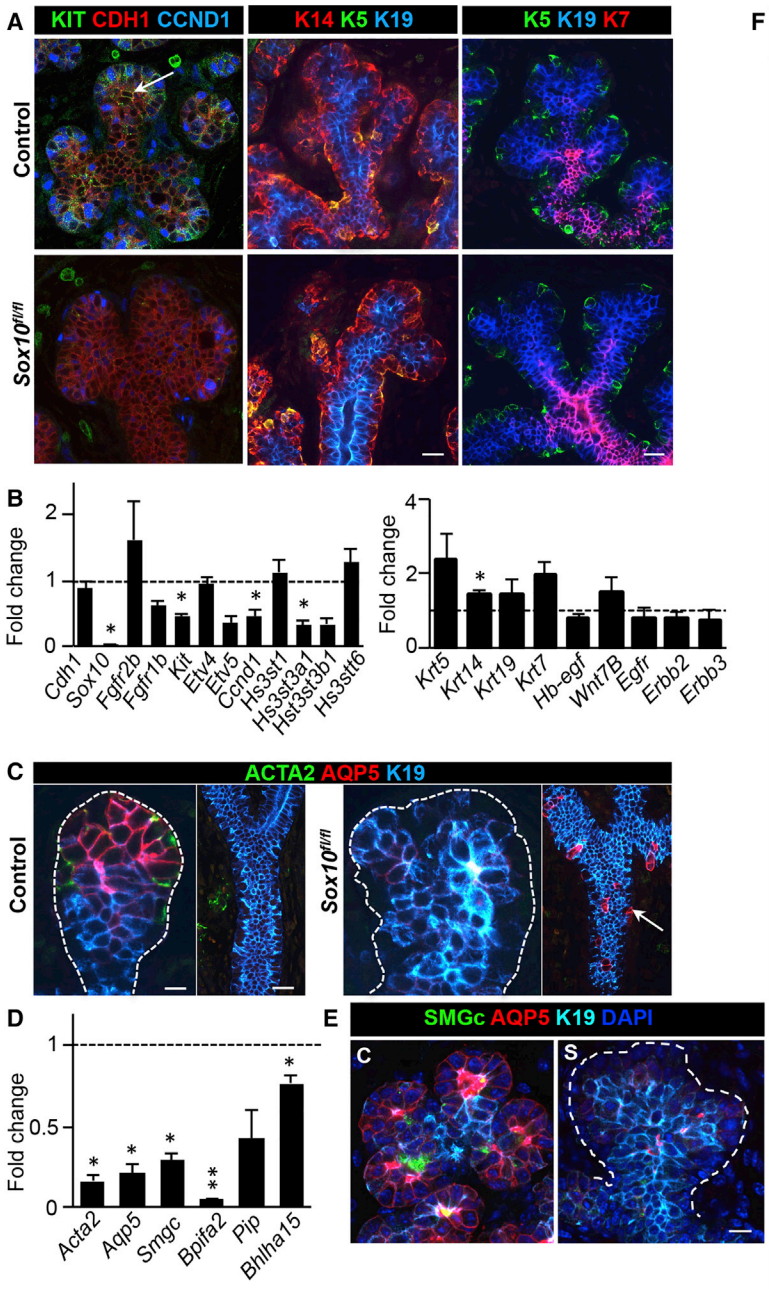

F

Gene	- Log2 F.C.	P-value
Rps15a-ps8	8.92	9.02E-03
Rps13-ps1	8.44	1.12E-02
Alox12e	8.08	1.17E-05
Ftl2	7.43	1.81E-02
C130046K22	7.00	6.33E-08
Bpifa2	4.52	1.80E-17
Dcpp3	3.10	1.23E-09
Cnn1	2.73	1.51E-03
Bpifb5	2.63	8.57E-03
Nipal4	1.90	3.94E-02
Myh11	1.85	7.34E-04
Cpm	1.42	1.33E-07
Col9a1	1.41	7.75E-28
Ttpa	1.31	1.59E-03
Aqp5	1.20	4.80E-05
Ccny	0.92	3.41E-24
Lcn2	0.89	6.84E-12
Sox10	0.88	9.26E-12
Cldn1	0.77	1.01E-09
Vwa2	0.77	3.38E-09
Aim1	0.74	1.14E-03
Actg2	0.71	4.68E-09
Kcnn4	0.71	3.05E-08
Tagln	0.71	1.06E-08
Shisa8	0.68	5.22E-10
Dcpp1	0.67	3.70E-09
BC006965	0.64	8.13E-07
AY036118	0.63	2.40E-07
Aldoc	0.62	1.54E-06
Ano1	0.61	9.65E-07
Galnt3	0.60	3.46E-06
Crispld2	0.59	5.52E-08
Myl9	0.58	1.18E-06
Adamts18	0.57	1.63E-06
Igfbp2	0.56	8.75E-06
Elf5	0.56	1.73E-05
ab	0.54	4.48E-06
Rgr	0.54	3.83E-06
Spon1	0.54	4.71E-12
Ccnd1	0.53	1.24E-05
Chn2	0.53	4.19E-05
Ugt8a	0.52	2.11E-06
Tmem238	0.52	1.65E-05
Snora73b	0.51	1.79E-05
Acta2	0.51	9.57E-06
Chadl	0.51	7.94E-05
Nxf7	0.50	3.60E-05

Figure 4. *Sox10* Induces Plasticity By Regulating fetal KIT^{+} Progenitor Maintenance and Differentiation

(A) Confocal imaging of control and *Sox10*$^{fl/fl}$ E16 SMGs endbuds. Tissue was stained for KIT (arrow), CDH1, CCND1, K14, K5, K19, and/or K7. Scale bars, 20 μm.

(B) Graphs show fold changes in gene expression of the *Fgfr2b/Kit* signaling pathway in epithelial (*Cdh1*) cells of *Sox10*$^{fl/fl}$ E16 SMGs, *Ccnd1*, heparan sulfates, as well as ductal-related markers (*Krt*'s) and correlated signaling pathways (*Egf*, *Wnt*). Data were normalized to *Rps29* and control (dotted line). Mean ± SEM, N > 3, multiple comparison t test. *p < 0.05.

(C) Confocal imaging of stained E16 control and *Sox10*$^{fl/fl}$ SMGs with ACTA2, AQP5, and K19. Arrow represents mislocated AQP5 expression in ducts. Scale bars, 20 μm.

(D) Fold changes in gene expression of proteins expressed by myoepithelial, acinar, and/or ID cells. Data was normalized to *Rps29* and control (dotted line). Mean ± SEM, N > 3, multiple comparison t test. *p < 0.05. **p < 0.01.

(legend continued on next page)

intercalated duct, and myoepithelial cells begins, and continues up to post-natal day 20 (Larsen et al., 2011). The pro-acinar and intercalated duct cells both express AQP5 and are surrounded by an outer layer of myoepithelial cells (Figure 4C). This differentiation process only occurs in distal endbuds and not in the ducts. Consistent with our hypothesis, ACTA2 and AQP5 were absent in distally located cells of *Sox10*$^{fl/fl}$ SMGs (Figure 4C). Moreover, acinar-specific secretory proteins, such as *Bpifa2* (parotid secretory protein, *Psp*), submandibular gland protein C (*Smgc*), and TF *Bhlha15* (Mist1) were downregulated (Figures 4D and 4E), illustrating a loss in initial differentiation of multiple cell types comprising the secretory unit of adult glands. Surprisingly, AQP5^{+} cells emerged proximally along the ducts of *Sox10*$^{fl/fl}$ SMGs (Figure 4C), suggesting a potential compensation mechanism of the remaining *Sox10*$^{fl/fl}$ ducts to differentiate into AQP5^{+} pro-acinar and/or intercalated duct (ID) cells.

Next, we performed RNA sequencing on E16 control and *Sox10*$^{fl/fl}$ SMGs to identify molecular pathways related to *Sox10* in organ development. We obtained expression profiles from independent ($N \geq 3$) biological samples and identified 81 genes that were downregulated more than −0.25 log2-fold change in *Sox10*$^{fl/fl}$ SMGs (Figures 4F and S4E). We used qPCR to validate *Sox10*, *Aqp5*, *Ccnd1*, *Bpifa2*, and *Acta2*. The set of downregulated genes were generally epithelial cell specific, as suggested by the mouse gene atlas network (Enrichr program [Chen et al., 2013], Figure S4F). Kyoto Encyclopedia of Genes and Genomes network pathway analysis identified downregulated genes as part of the vascular smooth muscle contraction, focal adhesion, and tight junction pathways (Figure S4G). Genes in cGMP-PKG signaling reflect decreases in pathways using intracellular cGMP-dependent physiological processes that may show alterations of cytosolic calcium concentrations. Also associated with this is the neuropeptide oxytocin pathway, which is mediated via the oxytocin receptor, and exerts stimulation of milk release during lactation and myoepithelial contraction (Crowley, 2015). Other genes are related to the overall salivary secretion and hormone release/secretory protein synthesis, including prolactin signaling, mucin type O-glycan biosynthesis, glycolysis/gluconeogenesis, and insulin secretion. Overall, these results indicate a regulatory network by which *Sox10* stimulates KIT-dependent maintenance and their initiation toward multiple cell types of the secretory unit.

Non-SOX10^{+} Adult Duct Progenitors Fail to Initiate Proper Secretory Organ Function

While the loss of *Sox10* during development reduced secretory unit differentiation, we predicted that post-natal salivary glands would also have reduced secretory function. A significant decrease was noticed in adult SMG size and weight in both sexes (Figures 5A and 5B and S5A). Although the SLG weight was not affected, which is expected since its development has been shown to be SOX2 dependent (Emmerson et al., 2017), we examined adult male and female SMGs via H&E staining, which showed disrupted cellular morphology. Acinar (Ac), ID, SD, and granular convoluted tubule cells are well defined in controls based on nuclear/cytoplasmic deposition, but their unique characteristics were not visible in *Sox10*$^{fl/fl}$ SMGs (Figures 5C and S5A). Cells became disorganized within the SMG, and some ductal structures were observed. The epithelial compartment of the adult SMG showed aberrant morphology, with an apparent increase in the amount of blood vessels (PECAM1, P1) and neuronal cells (TUBB3) (Figure 5D). mRNA analysis via qPCR confirmed increased trends of neuronal *Tubb3* and *Gfra2* (Figure 5E). Interestingly, changes in the mesenchymal and neuronal microenvironment were not noticeable during developmental stages E13 and E16 (Figures S5B and S5C). The parasympathetic ganglia (TUBB3^{+}) remained closely associated with the main duct, appeared similar in size, and innervated the endbuds similar to control. In addition, endothelial networks (PECAM1^{+}) and stromal (*Cdh11*) cells appeared similar to control, suggesting that loss of the secretory units does not affect innervation or blood vessel formation.

Next, we investigated the cell fate of remaining epithelial cells in adult *Sox10*$^{fl/fl}$ SMGs. As predicted, *Sox10*$^{fl/fl}$ SMGs had fewer secretory units and significantly more ducts (K19^{+}, white dotted line) that were, surprisingly, surrounded by non-duct epithelia (CDH1^{+} K19^{-}, yellow dotted line) (Figure 5D). However, only a few of the non-ductal epithelial cells expressed adult acinar-specific TF BHLHA15 (MIST1), AQP5, and/or secretory mucin protein MUC10 (Figures 5D and 5E). Interestingly, while the overall protein expression of AQP5 decreased (Figure 5D), its specific apical expression on the cells was reduced and the membrane localization remained limited only to the lateral border (Figure S5D). The absence of apical AQP5, as seen in control SMGs (Larsen et al., 2011), would be predicted to reduce fluid secretion. In addition, using qPCR, there was a reduction in the mRNA expression of other

(E) *Sox10*$^{fl/fl}$ and control E16 SMGs were stained for SMGc, AQP5, K19, and DAPI and analyzed by confocal microscopy. Dotted line outlines the distal area. Scale bar, 20 μm.

(F) RNA sequencing data of E16 *Sox10*$^{fl/fl}$ SMGs versus control. The list of downregulated genes was generated after bioinformatic analysis of next-generation sequencing data and cutoff at log2 fold change (FC) of −0.25. Genes outlined in bold were validated by qPCR analysis.

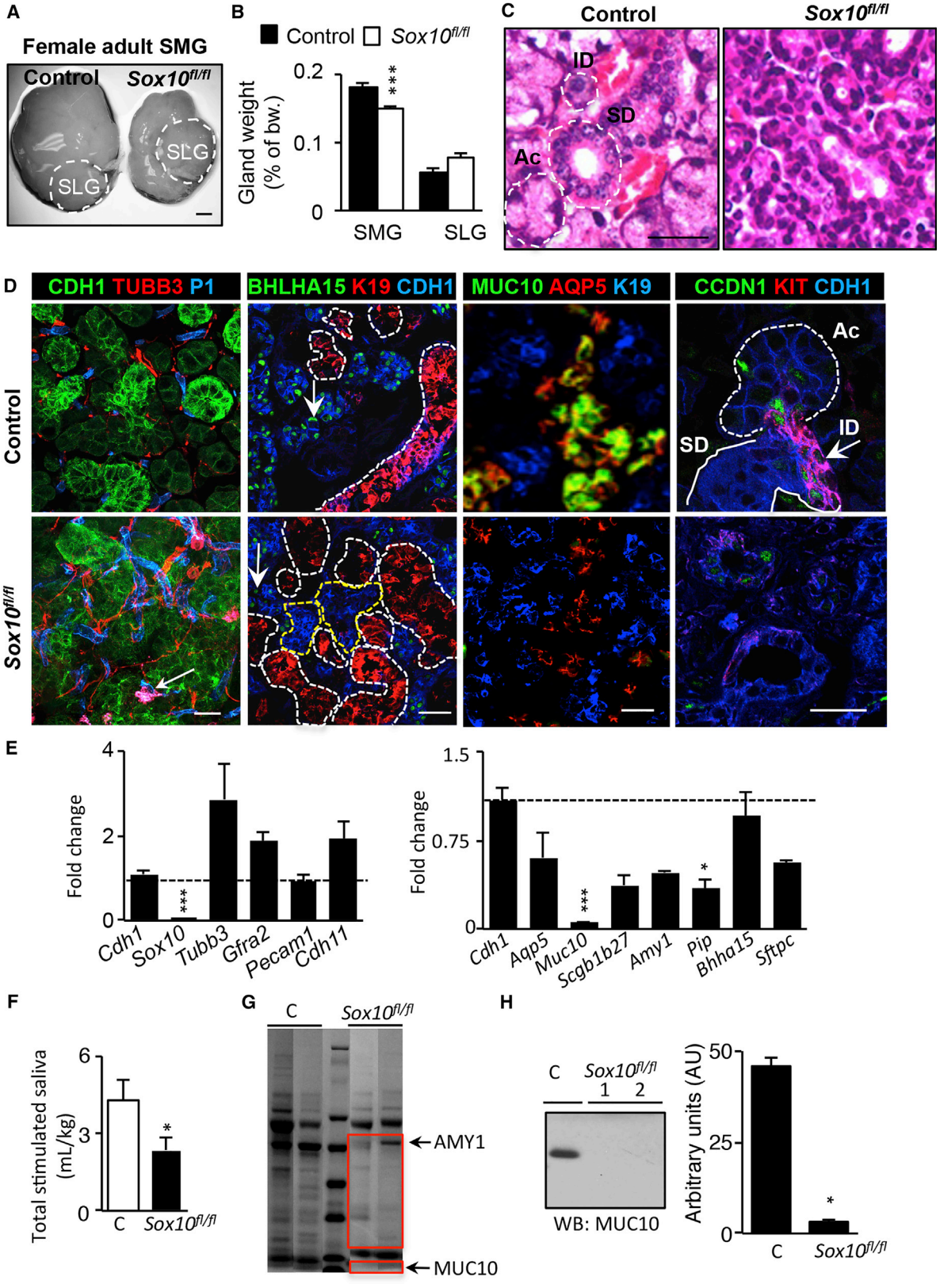

(legend on next page)

secretory proteins observed that are produced by acinar cells, including Secretoglobin b1b27 (*Scgb1b27*, *Abpa*), amylase-1 (*Amy1*), prolactin-induced protein (*Pip*), and surfactant-associated protein C (*Sftpc*) (Figure 5E).

Importantly, adult epithelial cells that did not fully differentiate into secretory unit cells were confirmed to be the progeny of *Krt14*-Cre;*Sox10*$^{flox/flox}$ cells, as all adult epithelia expressed mGFP (Figure S5E). To outline ID cells, we analyzed KIT expression. Typical KIT$^+$ ID cells were absent in *Sox10*$^{fl/fl}$ SMGs, and overall proliferation (*Ccnd1*) was reduced (Figure 5D). In contrast, myoepithelial cells co-expressing ACTA2, K14, and K5 were more abundant in *Sox10*$^{fl/fl}$ SMGs, surrounding the prominent ductal compartment (Figure S5F). Interestingly, these data suggest that non-*Sox10* duct cells also have the potential to form myoepithelial cells in the absence of KIT$^+$SOX10$^+$ progenitors, suggesting a second source of myoepithelial progenitors.

To confirm the secretory deficiency of the *Sox10*$^{fl/fl}$ SMGs, we measured total saliva production after pilocarpine stimulation, which includes secretions from SMG, PAR, and SLGs. We measured ~50% reduction in saliva, likely reflecting reduced PAR and SMG function, since the SLGs appeared unaffected by loss of *Sox10* (Figure 5F, N ≥ 4). Subsequently, protein analysis of the saliva by SDS-PAGE and Coomassie staining highlighted that there are quantitative differences in salivary proteins (e.g., AMY1), as well as in low-molecular-weight proteins (Figure 5G, red box). Western blot analysis of an acinar-specific mucin, MUC10, confirmed its loss in saliva (Figure 5H). Overall, these observations suggest that the remaining non-*Sox10* duct cells attempt to compensate for the loss in secretory unit formation. However, in the adult environment the duct cells cannot alter their fate to form functional secretory units, which reduces organ function.

In a similar manner, the MMGs of lactating *Sox10*$^{fl/fl}$ mice were smaller and showed white discoloration (Figure S5G). Morphologically, *Sox10*$^{fl/fl}$ MMGs showed few to no secretory units, which normally consist of ductal (KRT8$^+$CDH1$^+$), alveolar (KRT8$^-$CDH1$^+$), and myoepithelial (ACTA2$^+$) cells. In addition, pups from *Sox10*$^{fl/fl}$ mice did not survive the first 24 h post-birth unless fostered by control mice, confirming the inability of MMGs in adult *Sox10*$^{fl/fl}$ mice to properly produce milk.

Overall, these data indicate that the effects of SOX10 loss affect multiple branching organs in their secretory function.

Expression of *Sox10* Increases Plasticity of Ductal Cells and Drives KIT$^+$ Progenitor Formation

In complementary *in vitro* and *ex vivo* experiments, we used virus-mediated overexpression of *Sox10* in a mouse and human cell line and in primary mouse fetal cells as proof-of-principle experiments to determine *Sox10*'s capacity to alter the cell fate in non-KIT duct cells. We first transfected mouse salivary gland epithelial duct (SIMS) and human adult MMG luminal duct (MCF10A) cell lines. Cells were transduced with lentivirus particles expressing *Sox10* with human influenza hemagglutinin tag (*Sox10-HA*), a mutated *Sox10* that did not generate SOX10 protein (Figure S6A) and/or CMV-*mCherry*. There was ~97% infection efficiency, which was confirmed on protein level after transduction with the SOX10$^+$-mCherry$^+$ vector, the empty-CMV-*mCherry* vector, or the mutated *Sox10*-CMV-mCherry vector by immunofluorescence and western blot quantification (Figures S6A–S6C). The mCherry fluorescence was enhanced by RFP staining, which detected all mCherry$^+$ cells (Figure S6B). Interestingly, after transduction with *Sox10* there was a significant increased gene expression of *Kit* in MCF10A and SIMS cells (Figures 6A and 6B). *Ffgr2b* was significantly upregulated in MCF10A and showed an increased trend in SIMS, as well as its downstream target *Etv4*. However, genes related to differentiation, such as *Acta2*, *Aqp5*, and/or *Amy1* remained unaltered during the limited time of passaging. Thus, in a minimal environment

Figure 5. *Sox10* Induces Plasticity by Regulating Fetal KIT$^+$ Progenitor Maintenance and Differentiation

(A) Bright-field picture of SMGs from female adult control or *Sox10*$^{fl/fl}$ mice. Scale bar, 1 mm.

(B) Graph represents weight of female SMGs as a percentage of body weight (bw) (control, 0.18% ± 0.01%; *Sox10*$^{fl/fl}$, 0.13% ± 0.02%). Female SLG (control, 0.06% ± 0.01%; *Sox10*$^{fl/fl}$, 0.07% ± 0.01%). Mean ± SEM, N > 3, unpaired t test. ***p < 0.005.

(C) H&E staining on paraffin sections of adult female SMGs of control or *Sox10*$^{fl/fl}$ mice. Ac, ID, and SDs are outlined by white dotted line. Scale bar, 25 μm.

(D) Confocal imaging of adult control and *Sox10*$^{fl/fl}$ SMGs stained for CDH1, TUBB3, PECAM1 (P1), BHLHA15, K19, MUC10, AQP5, KIT, and CCND1. Scale bars, 20 μm.

(E) qPCR analysis of genes comparing adult control and *Sox10*$^{fl/fl}$ SMGs. Mean ± SEM, N > 3, multiple comparison t test. ***p < 0.001, *p < 0.05.

(F) Saliva production of adult control and *Sox10*$^{fl/fl}$ mice, normalized to their body weight. Mean ± SEM, N > 3, unpaired t test. *p < 0.05.

(G) Secretory proteins from saliva of adult control and *Sox10*$^{fl/fl}$ mice were separated using SDS-PAGE. Gels were stained with Coomassie blue.

(H) MUC10 protein analysis in saliva of adult control and *Sox10*$^{fl/fl}$ mice via western blot (WB). Graph shows quantification of MUC10 western using densitometry analysis. Mean ± SEM, N ≥ 3, unpaired t test. *p > 0.05.

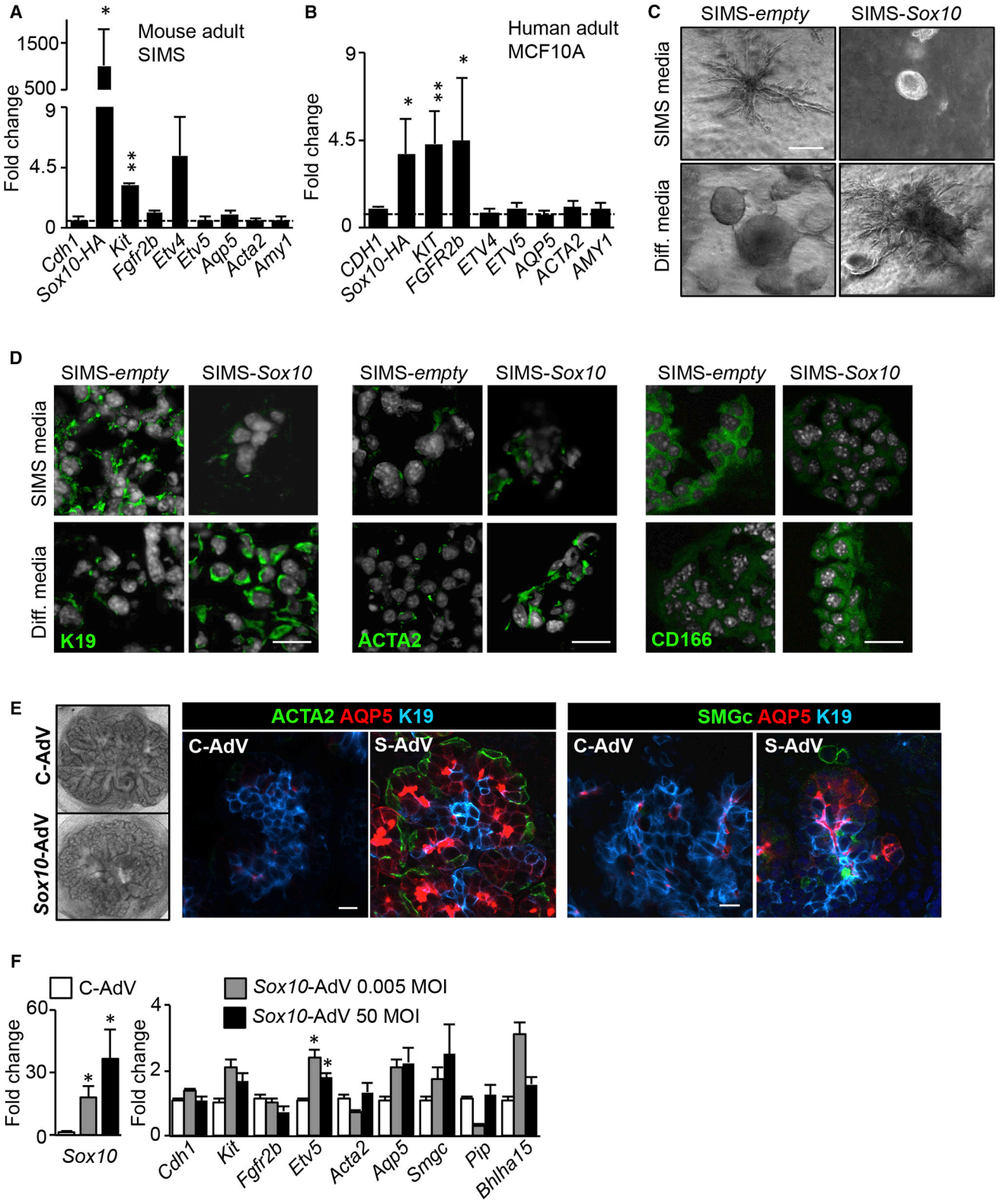

Figure 6. *Sox10* Induces Plasticity by Regulating Fetal KIT$^+$ Progenitor Self-Renewal and Differentiation

(A and B) Fold changes in gene expression of SIMS and MCF10A transduced with lentivirus-expressing *Sox10*, grown in 2D. Data were normalized to empty lentivirus-transduced cells and *Rps29* (dotted line). Mean ± SEM, N > 3, multiple comparison t test. *p < 0.05. **p < 0.01.

(legend continued on next page)

of 2D epithelial cell culture, *Sox10* expression can induce KIT$^+$FGFR2b$^+$SOX10$^+$ cell-like type in adult ductal cells.

As proper secretory unit formation may require 3D settings, we placed SIMS-*empty* or SIMS-*Sox10* cells in 3D. We used SIMS medium, as used in 2D, or differentiation medium, to stimulate secretory unit formation (Figures 6C, 6D, S6D, and S6E). By 7 days in SIMS medium, SIMS-*empty* cells showed branched structures containing K19$^+$ duct cells and cells expressing CD116, a marker for adult acinar cells (Maria et al., 2012). In contrast, SIMS-*Sox10* cells formed round spheroids consisting of cells with low protein expression of K19, ACTA2, or CD166, suggesting that *Sox10* prevents differentiation. However, the opposite outcome was observed in differentiation medium. SIMS-*empty* cells grew as round spheroids with cells expressing low levels of K19, ACTA, and CD166, whereas SIMS-*Sox10* cells formed organoid-like structures with K19$^+$ ductal, ACTA2$^+$ myoepithelial, and CD166$^+$ acinar cells. Thus, while SOX10$^-$ SIMS-*empty* cells are able to form ducts and/or acini in 3D, overexpression of *Sox10* enables either cell maintenance or enhances differentiation into all secretory unit cell types. Moreover, this *Sox10*-driven cell fate decision seems to be dictated by different growth factors.

To evaluate whether *Sox10* alone can induce plasticity of fetal KIT$^+$SOX10-primary duct cells, we enzymatically isolated E13 epithelia of control and *Sox10$^{fl/fl}$* SMGs and transduced them with adenovirus (Adv)-expressing mouse *Sox10*. The fetal SMG is easily dissociated into epithelium and mesenchyme, which is the endogenous fetal microenvironment containing stromal, endothelial, and neuronal cells. These compartments can be genetically manipulated with viral vectors before they get recombined and cultured further. Adv-*eGFP* was used as a control to show the high transduction efficiency of Adv in SMG epithelia (Figure S6F). Consequently, transduced epithelia were recombined with mesenchyme and cultured *ex vivo* for 6 days to reach an E16 SMG equivalent stage, as determined by the expression of cellular differentiation markers of myoepithelial, Ac, and ID cells (Figure S6G). Recombined *Sox10$^{fl/fl}$* SMGs treated with control Adv had a ductal morphology, while *Sox10*-Adv treated explants formed prominent endbuds (Figures 6E and S6H). Two different doses of Adv were used; MOI 0.005 and 50. Both MOIs resulted in increased expression of *Sox10* ~20–40-fold, and qPCR analysis also showed increased expression of *Kit*, *Etv5*, *Aqp5*, *Smgc*, and *Bhlha15* (Figure 6F). Thus, gene expression changes suggested there was increased secretory unit differentiation with *Sox10* overexpression. Immunostaining highlighted a striking change in endbud morphology. There was a reappearance of distally located ACTA2$^+$ myoepithelial, AQP5$^+$ acinar/ID cells, and SMGc$^+$ acinar cells (Figure 6E), which confirmed that *Sox10* is sufficient to induce cell fate changes in fetal non-KIT duct cells and regain the characteristics of multi-potent KIT$^+$SOX10$^+$ progenitors in a normal developing environment.

Overall, these data indicate that expression of the TF *Sox10* can induce plasticity to form KIT$^+$SOX10$^+$ progenitors in adult epithelial duct cells. Moreover, in 3D *ex vivo* settings, *Sox10* expression increases the plasticity of non-SOX10 expressing duct cells to either induce maintenance or differentiation into secretory units.

DISCUSSION

Our studies have identified an essential role for *Sox10* in the formation of multi-potent progenitors within multiple exocrine glands. First, *Sox10* is essential for the maintenance and proliferation of KIT$^+$ progenitors. An additional role of *Sox10* is to initiate the differentiation of KIT$^+$ progenitors toward myoepithelial, acinar, and ID cells, all of which form the secretory unit of exocrine glandular tissues. Lastly, we show that *Sox10* expression can alter the plasticity of non-KIT epithelial cells by driving their cell fate toward a multi-potent KIT$^+$ progenitor; all which indicate that SOX10 is a universal master regulator in exocrine glands.

There are striking similarities in the role of *Sox10* in multiple exocrine glands. Our initial findings that *Sox10* is regulated by KIT/FGFR2b signaling (Lombaert et al., 2013) was later, in part, confirmed in both lacrimal and MMGs (Chen et al., 2014; Dravis et al., 2015), in which FGF10/FGFR2b activation or loss influenced *Sox10* expression. We show that KIT and SOX10 are present in distal lacrimal gland endbuds. Similarly, both SOX10 and KIT expression were correlated with mammary epithelial progenitors (Dravis et al., 2015; Regan et al., 2012).

(C) Bright-field pictures of SIMS-*empty* or SIMS-*Sox10* in 3D, and cultured for 7 days in SIMS medium or differentiation (diff) medium. Scale bar, 250 μm.

(D) Confocal images of K19, ACTA2, and CD166 on cells in the various conditions seen in (C). Scale bars, 30 μm.

(E) Bright-field pictures of recombined fetal SMGs. Control or *Sox10$^{fl/fl}$* SMG E13 epithelia was transfected with control eGFP-Adv (C-Adv) or *Sox10*-Adv (S-Adv) at 0.005 or 50 MOI before being recombined with its original mesenchyme, blood vessels, and parasympathetic ganglia. Recombined glands were cultured for an additional 6 days. Tissue was stained for ACTA2, AQP5, K19, or SMGc, and analyzed by confocal microscopy. Scale bars, 20 μm.

(F) Fold changes in expression of *Sox10*, and genes related to *Fgfr2b/Kit* signaling, myoepithelial, acinar, and ID markers from tissue in (E). Data were normalized to *Rps29* and C-Adv recombined tissue. Mean ± SEM, N > 3, multiple comparison t test. *p < 0.05.

Also, *in vitro* mammary spheroid assays determined that SOX10$^+$ stem/progenitors were three times more potent than the classical CD24^{hi}CD49f$^+$ cells, which long defined MMG stem cells (Dravis et al., 2015). In addition, SOX10$^+$ tumors from both salivary (Ohtomo et al., 2013) and MMGs (Hsieh et al., 2016) show characteristics of acinar, ID, and/or myoepithelial cells. Together with our data showing that SOX10 marks multi-potent progenitors during the initiation of lacrimal and salivary glands, we conclude that *Sox10* is a master regulator of secretory unit differentiation in multiple exocrine glands.

The function of *Sox10* correlates to its expression levels (Dravis et al., 2015). For example, ectopic *Sox10* overexpression in isolated primary mammary organoids results in a mesenchymal-like phenotype. The high expressing *Sox10* cells failed to organize into secondary organoids, whereas lower *Sox10* levels enabled the formation of secondary organoids. In contrast, our ectopic expression experiments were performed by *ex vivo* recombination assays allowing the *Sox10*-transduced epithelium to interact with its endogenous multi-cell fetal microenvironment. We concluded that *Sox10* expression drives the formation of the KIT$^+$SOX10$^+$ progenitor state, which can differentiate into multiple cell types. Even at high *Sox10* expression levels, myoepithelial cell differentiation occurs, which involves an epithelial-mesenchymal transition in glandular tissues (Zhao et al., 2012). Myoepithelial cells in the MMG share a transcriptional profile with a breast cancer subtype, which was proposed to derive from a highly migratory myoepithelial progenitor (Zhao et al., 2012). These data are thus not contradictory with our results, as plasticity is defined by both cell-autonomous and non-cell-autonomous settings. The microenvironment therefore plays a critical role in the level to which plasticity is induced. Both studies cultured mammary myoepithelial progenitors or *Sox10*-expressing epithelial cells in Matrigel, a basement membrane extract, which resulted in loss of polarization and elevated migratory properties. Our data show how *Sox10* overexpression in non-*Sox10* fetal epithelial cells cultured in their endogenous multi-cell-type fetal microenvironment results in epithelial differentiation. This endogenous 3D fetal tissue microenvironment is as important to direct cell plasticity as the intracellular master regulator(s). Secreted factors from other cell types may be required in combination with *Sox10* to induce plasticity and direct the various cell lineages in normal, deprived, diseased, or injured environments. This idea is supported by the fact that *Sox10* overexpression in adult duct cells in 2D induced plasticity toward a KIT-like cell, but drove maintenance or differentiation in 3D settings. However, we speculate that *Sox10* might need additional master regulators to induce plasticity in cells that are of a more distant cell lineage.

An interesting finding in our study was the inability of remaining epithelial duct cells in *Sox10$^{fl/fl}$* SMGs to differentiate into functional secretory units. Multiple progenitors have been identified that participate during salivary gland development. At various time-points during organogenesis multi-potent and more restricted progenitors are formed. One late-stage bipotent progenitor expressing TF *Ascl3* is detected in the SMG at E16. From lineage-tracing studies, *Ascl3* cells give rise to some, but not all, adult ductal and mucous-secreting acinar cells (Bullard et al., 2008). Ablation of *Ascl3* cells did not reveal any impact on glandular formation, likely due to compensation of other progenitors present (Arany et al., 2011). In contrast, loss of KIT progenitors by reducing *Sox10* had a great impact on gland morphology. Surprisingly, higher *Ascl3* expression was observed at E16. Yet, *Ascl3*-expressing cells and/or other non-KIT progenitors were not sufficient to produce fully functional secretory units. Interestingly, myoepithelial cell formation did occur from non-KIT duct progenitors, which supports a novel concept that myoepithelial cells can arise from two independent cell sources; KIT$^+$ progenitors and non-KIT progenitors.

Another issue requiring further investigation is whether an altered microenvironment is created after loss of KIT$^+$ progenitors and their immediate progeny post-E16. Multi-cell-type crosstalk occurs between glandular epithelial progenitors, neuronal, stromal, and endothelial cells (Kwon et al., 2017; Lombaert, 2017). It is possible that the absence of KIT$^+$ progenitors and their progeny affects paracrine signals that influence blood vessel and neuronal cell formation. The control of secretory function in adult tissues is dependent on innervation. Whether lack of secretory units influences the amount or type of innervation remains to be investigated. It also remains to be tested whether SOX10$^-$ duct cells can form mature acinar cells postnatally in a SOX10-independent manner. Similarly, it still needs to be determined whether SOX10 regulates the expression of *Kit* and *Fgfr2b* directly or indirectly. At a minimum, our data suggest that SOX10 plays a role in the positive feedback loop of KIT/FGFR2b signaling.

In conclusion, our results suggest that *Sox10* is a master regulator in epithelial KIT$^+$ progenitors of exocrine glands, including lacrimal, salivary, and MMGs, thus making it a potential target to induce secretory unit formation for *in vitro* glandular tissue engineering purposes and/or regenerative strategies.

EXPERIMENTAL PROCEDURES

Animal Care and Use

All experiments were approved by the animal care and use committees at the University of Michigan and the National Institute

of Dental and Craniofacial Research at the NIH. More information is given in the Supplemental Information.

Ex Vivo Organ Culture, Recombination Assays, and Adenovirus Transduction

Isolation of fetal tissue, epithelial dissection, fetal tissue culture, growth factor concentrations, and recombination assays were described previously (Lombaert et al., 2013). More information is given in the Supplemental Information.

Immunohistochemistry/Fluorescence

Fetal tissue was fixed, blocked, stained, and labeled with primary antibodies according to previously described protocols (Lombaert et al., 2013). More information is given in the Supplemental Information.

qPCR

Real-time PCR was performed as described previously (Lombaert et al., 2013). More information is given in the Supplemental Information.

Saliva Collection

Animals were placed in a restraining device 5 min after pilocarpine injection (2.5 mg/kg, subcutaneously). Saliva was then collected for 15 min and quantified as a volume to body weight ratio, as outlined in (Lombaert et al., 2008). More information is given in the Supplemental Information.

Western Blot Analysis and Coomassie Staining

Protein from saliva was quantified with a BCA test, and resolved on Bis-Tris gels. More information is given in the Supplemental Information.

RNA Sequencing and Bioinformatics Analysis

Total RNA was extracted from E16 SMGs using the Ambion microRNA kit. More information is given in the Supplemental Information.

Lentiviral Overexpression and 3D Culture

SIMS and MCF10a cells were cultured and grown in their respective growth media (Laoide et al., 1996; Qu et al., 2015). More information is given in the Supplemental Information.

Statistical Analysis and Data Availability

Statistical parameters included $N \geq 3$. More information is given in the Supplemental Information.

ACCESSION NUMBERS

The accession number for the RNA-seq data reported in this paper is GEO: GSE123341.

SUPPLEMENTAL INFORMATION

Supplemental Information includes Supplemental Experimental Procedures and six figures and can be found with this article online at https://doi.org/10.1016/j.stemcr.2019.01.002.

AUTHOR CONTRIBUTIONS

H.K.A., G.M., E.T., A.C., E.H., K.Y., and E.B. performed the experiments and analyzed the data. M.P.H. and I.M.A.L. conceptualized the project. I.M.A.L. designed, coordinated the work, and wrote the article. All authors revised the manuscript for intellectual content, agreed to be accountable for all aspects of the work, and gave final approval for submission.

ACKNOWLEDGMENTS

This work was supported by NIH R00 DE022557 grant and the Intramural Program of the National Institute of Dental and Craniofacial Research at the NIH. We thank Dr. Wegner for providing the *Sox10*$^{fl/fl}$ mice, and Drs. Robert Morell and Daniel Martin of the NIDCR/NIDCD Genomics and Computational Biology Core for the RNA sequencing data and the NIDCR Veterinary Resources Core at NIH.

Received: May 3, 2018
Revised: December 31, 2018
Accepted: January 2, 2019
Published: January 31, 2019

REFERENCES

Abdelalim, E.M., Emara, M.M., and Kolatkar, P.R. (2014). The SOX transcription factors as key players in pluripotent stem cells. Stem Cells Dev. *23*, 2687–2699.

Arany, S., Catalan, M.A., Roztocil, E., and Ovitt, C.E. (2011). Ascl3 knockout and cell ablation models reveal complexity of salivary gland maintenance and regeneration. Dev. Biol. *353*, 186–193.

Avilion, A.A., Nicolis, S.K., Pevny, L.H., Perez, L., Vivian, N., and Lovell-Badge, R. (2003). Multipotent cell lineages in early mouse development depend on SOX2 function. Genes Dev. *17*, 126–140.

Bullard, T., Koek, L., Roztocil, E., Kingsley, P.D., Mirels, L., and Ovitt, C.E. (2008). Ascl3 expression marks a progenitor population of both acinar and ductal cells in mouse salivary glands. Dev. Biol. *320*, 72–78.

Chan, S.S., and Kyba, M. (2013). What is a master regulator? J. Stem Cell Res. Ther. *3*. https://doi.org/10.4172/2157-7633.1000e114.

Chatzeli, L., Gaete, M., and Tucker, A.S. (2017). Fgf10 and Sox9 are essential for the establishment of distal progenitor cells during mouse salivary gland development. Development *144*, 2294–2305.

Chen, E.Y., Tan, C.M., Kou, Y., Duan, Q., Wang, Z., Meirelles, G.V., Clark, N.R., and Ma'ayan, A. (2013). Enrichr: interactive and collaborative HTML5 gene list enrichment analysis tool. BMC Bioinformatics *14*, 128.

Chen, Z., Huang, J., Liu, Y., Dattilo, L.K., Huh, S.H., Ornitz, D., and Beebe, D.C. (2014). FGF signaling activates a Sox9-Sox10 pathway for the formation and branching morphogenesis of mouse ocular glands. Development *141*, 2691–2701.

Crowley, W.R. (2015). Neuroendocrine regulation of lactation and milk production. Compr. Physiol. *5*, 255–291.

Donati, G., and Watt, F.M. (2015). Stem cell heterogeneity and plasticity in epithelia. Cell Stem Cell *16*, 465–476.

Dravis, C., Spike, B.T., Harrell, J.C., Johns, C., Trejo, C.L., Southard-Smith, E.M., Perou, C.M., and Wahl, G.M. (2015). Sox10 regulates stem/progenitor and mesenchymal cell states in mammary epithelial cells. Cell Rep. *12*, 2035–2048.

Emmerson, E., May, A.J., Nathan, S., Cruz-Pacheco, N., Lizama, C.O., Maliskova, L., Zovein, A.C., Shen, Y., Muench, M.O., and Knox, S.M. (2017). SOX2 regulates acinar cell development in the salivary gland. Elife *6*. https://doi.org/10.7554/eLife.26620.

Hsieh, M.S., Lee, Y.H., and Chang, Y.L. (2016). SOX10-positive salivary gland tumors: a growing list, including mammary analogue secretory carcinoma of the salivary gland, sialoblastoma, low-grade salivary duct carcinoma, basal cell adenoma/adenocarcinoma, and a subgroup of mucoepidermoid carcinoma. Hum. Pathol. *56*, 134–142.

Jones, K.B., and Klein, O.D. (2013). Oral epithelial stem cells in tissue maintenance and disease: the first steps in a long journey. Int. J. Oral Sci. *5*, 121–129.

Knosp, W.M., Knox, S.M., and Hoffman, M.P. (2012). Salivary gland organogenesis. Wiley Interdiscip. Rev. Dev. Biol. *1*, 69–82.

Kwon, H.R., Nelson, D.A., DeSantis, K.A., Morrissey, J.M., and Larsen, M. (2017). Endothelial cell regulation of salivary gland epithelial patterning. Development *144*, 211–220.

Laoide, B.M., Courty, Y., Gastinne, I., Thibaut, C., Kellermann, O., and Rougeon, F. (1996). Immortalised mouse submandibular epithelial cell lines retain polarised structural and functional properties. J. Cell Sci. *109* (Pt 12), 2789–2800.

Larsen, H.S., Aure, M.H., Peters, S.B., Larsen, M., Messelt, E.B., and Kanli Galtung, H. (2011). Localization of AQP5 during development of the mouse submandibular salivary gland. J. Mol. Histol. *42*, 71–81.

Lo, H.G., Jin, R.U., Sibbel, G., Liu, D., Karki, A., Joens, M.S., Madison, B.B., Zhang, B., Blanc, V., Fitzpatrick, J.A., et al. (2017). A single transcription factor is sufficient to induce and maintain secretory cell architecture. Genes Dev. *31*, 154–171.

Lombaert, I., Movahednia, M.M., Adine, C., and Ferreira, J.N. (2017). Concise review: salivary gland regeneration: therapeutic approaches from stem cells to tissue organoids. Stem Cells *35*, 97–105.

Lombaert, I.M., Abrams, S.R., Li, L., Eswarakumar, V.P., Sethi, A.J., Witt, R.L., and Hoffman, M.P. (2013). Combined KIT and FGFR2b signaling regulates epithelial progenitor expansion during organogenesis. Stem Cell Reports *1*, 604–619.

Lombaert, I.M., Brunsting, J.F., Wierenga, P.K., Faber, H., Stokman, M.A., Kok, T., Visser, W.H., Kampinga, H.H., de Haan, G., and Coppes, R.P. (2008). Rescue of salivary gland function after stem cell transplantation in irradiated glands. PLoS One *3*, e2063.

Lombaert, I.M., and Hoffman, M.P. (2010). Epithelial stem/progenitor cells in the embryonic mouse submandibular gland. Front. Oral Biol. *14*, 90–106.

Lombaert, I.M., Knox, S.M., and Hoffman, M.P. (2011). Salivary gland progenitor cell biology provides a rationale for therapeutic salivary gland regeneration. Oral Dis. *17*, 445–449.

Lombaert, I.M.A. (2017). Implications of salivary gland developmental mechanisms for the regeneration of adult damaged tissues. In Salivary Gland Development and Regeneration, S. Cha, ed. (Springer), pp. 3–22.

Maria, O.M., Maria, A.M., Cai, Y., and Tran, S.D. (2012). Cell surface markers CD44 and CD166 localized specific populations of salivary acinar cells. Oral Dis. *18*, 162–168.

Ohtomo, R., Mori, T., Shibata, S., Tsuta, K., Maeshima, A.M., Akazawa, C., Watabe, Y., Honda, K., Yamada, T., Yoshimoto, S., et al. (2013). SOX10 is a novel marker of acinus and intercalated duct differentiation in salivary gland tumors: a clue to the histogenesis for tumor diagnosis. Mod. Pathol. *26*, 1041–1050.

Qu, Y., Han, B., Yu, Y., Yao, W., Bose, S., Karlan, B.Y., Giuliano, A.E., and Cui, X. (2015). Evaluation of MCF10A as a reliable model for normal human mammary epithelial cells. PLoS One *10*, e0131285.

Regan, J.L., Kendrick, H., Magnay, F.A., Vafaizadeh, V., Groner, B., and Smalley, M.J. (2012). c-Kit is required for growth and survival of the cells of origin of Brca1-mutation-associated breast cancer. Oncogene *31*, 869–883.

Reiprich, S., and Wegner, M. (2015). From CNS stem cells to neurons and glia: Sox for everyone. Cell Tissue Res. *359*, 111–124.

Rice, R., Spencer-Dene, B., Connor, E.C., Gritli-Linde, A., McMahon, A.P., Dickson, C., Thesleff, I., and Rice, D.P. (2004). Disruption of Fgf10/Fgfr2b-coordinated epithelial-mesenchymal interactions causes cleft palate. J. Clin. Invest. *113*, 1692–1700.

Rothova, M., Thompson, H., Lickert, H., and Tucker, A.S. (2012). Lineage tracing of the endoderm during oral development. Dev. Dyn. *241*, 1183–1191.

Tata, P.R., and Rajagopal, J. (2016). Cellular plasticity: 1712 to the present day. Curr. Opin. Cell Biol. *43*, 46–54.

Teshima, T.H., Wells, K.L., Lourenco, S.V., and Tucker, A.S. (2016). Apoptosis in early salivary gland duct morphogenesis and lumen formation. J. Dent. Res. *95*, 277–283.

Tucker, A.S. (2007). Salivary gland development. Semin. Cell. Dev. Biol. *18*, 237–244.

Wang, J., and Laurie, G.W. (2004). Organogenesis of the exocrine gland. Dev. Biol. *273*, 1–22.

Zhao, X., Malhotra, G.K., Band, H., and Band, V. (2012). Derivation of myoepithelial progenitor cells from bipotent mammary stem/progenitor cells. PLoS One *7*, e35338.

Stem Cell Reports, Volume *12*

Supplemental Information

Sox10 Regulates Plasticity of Epithelial Progenitors toward Secretory Units of Exocrine Glands

Harleen K. Athwal, George Murphy III, Ellis Tibbs, Ashley Cornett, Emily Hill, Kenji Yeoh, Elsa Berenstein, Matthew P. Hoffman, and Isabelle M.A. Lombaert

SUPPLEMENTAL FIGURES AND DATA

Sox10 Regulates Plasticity of Epithelial Progenitors towards Secretory Units of Exocrine Glands

Harleen K. Athwal[1,2,#], George Murphy III[1,2,#], Ellis Tibbs[3,#], Ashley Cornett[1,2], Emily Hill[1,2], Kenji Yeoh[1,2], Elsa Berenstein[3], Matthew P. Hoffman[3], Isabelle M.A. Lombaert[1,2,3,*]

SUPPLEMENTAL FIGURE 1

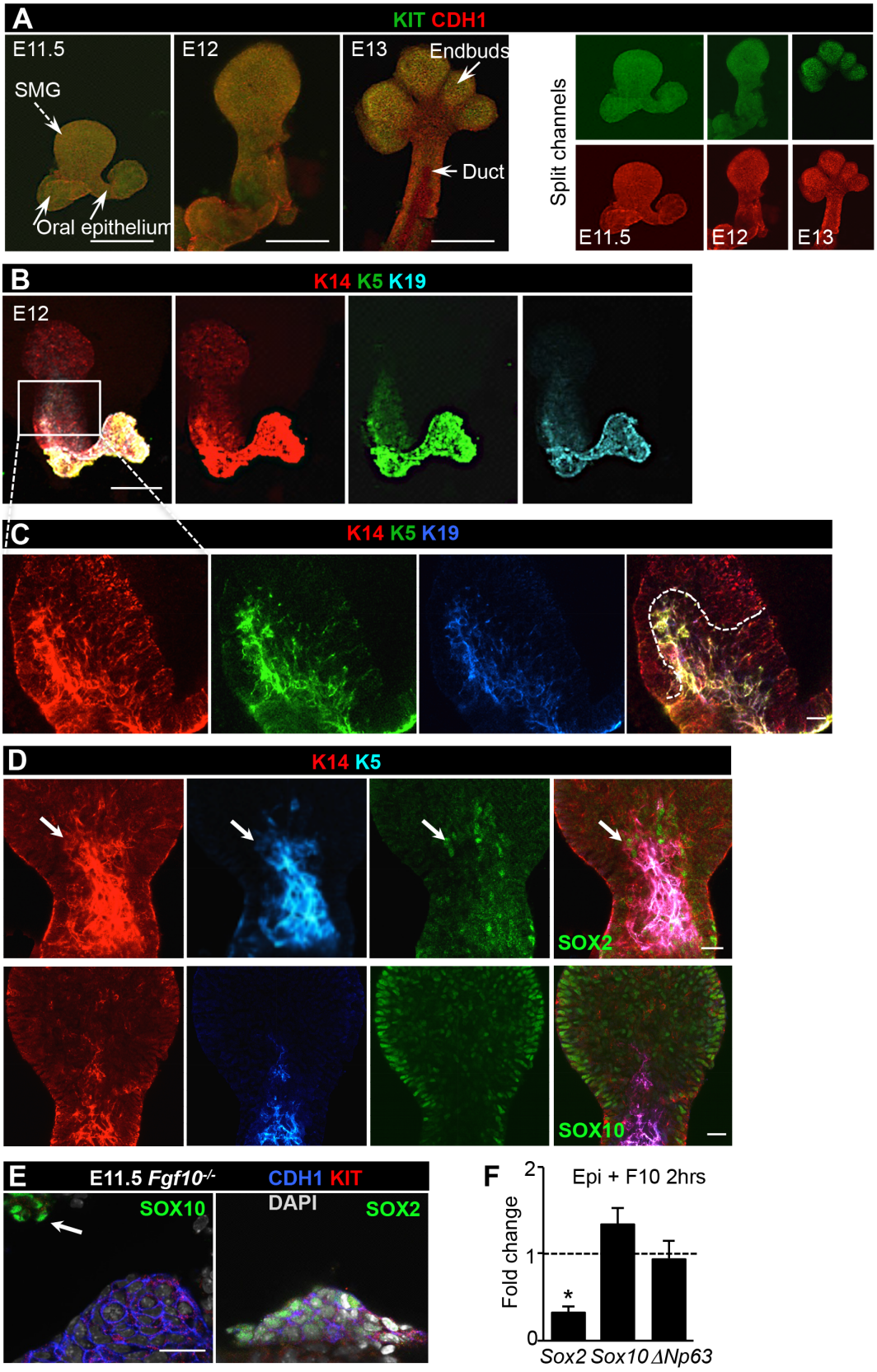

SUPPLEMENTAL FIGURE 2

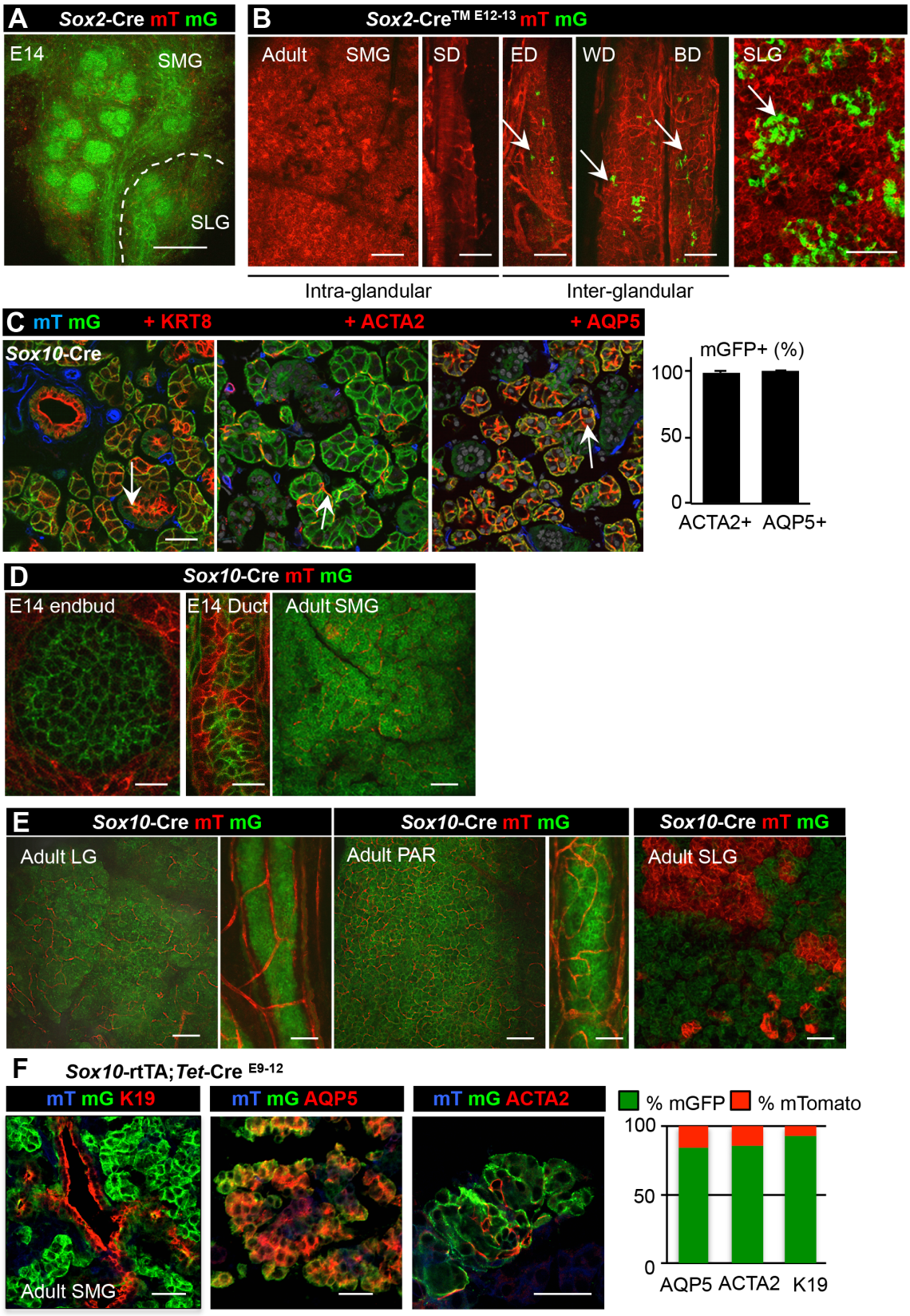

SUPPLEMENTAL FIGURE 3

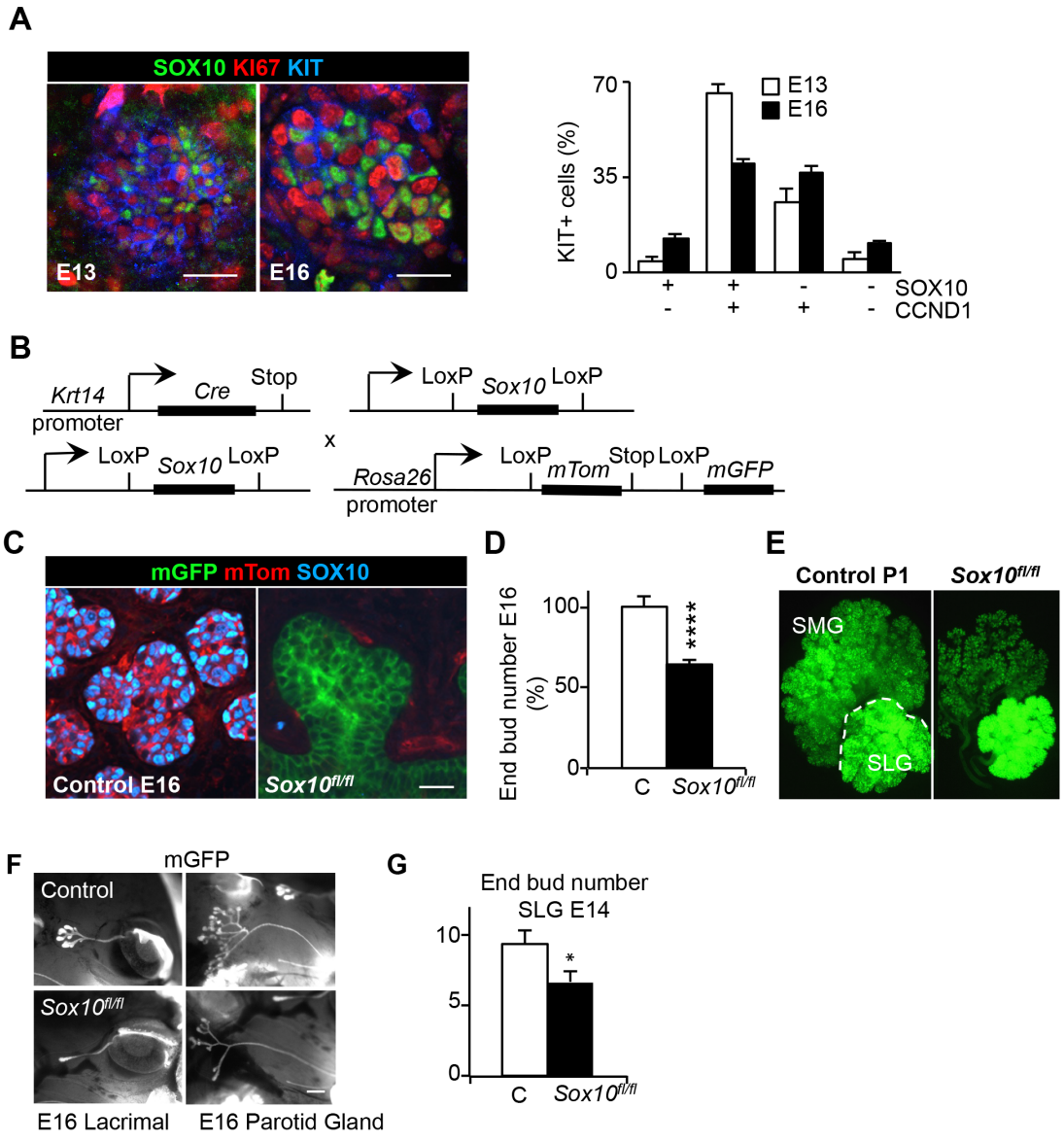

SUPPLEMENTAL FIGURE 4

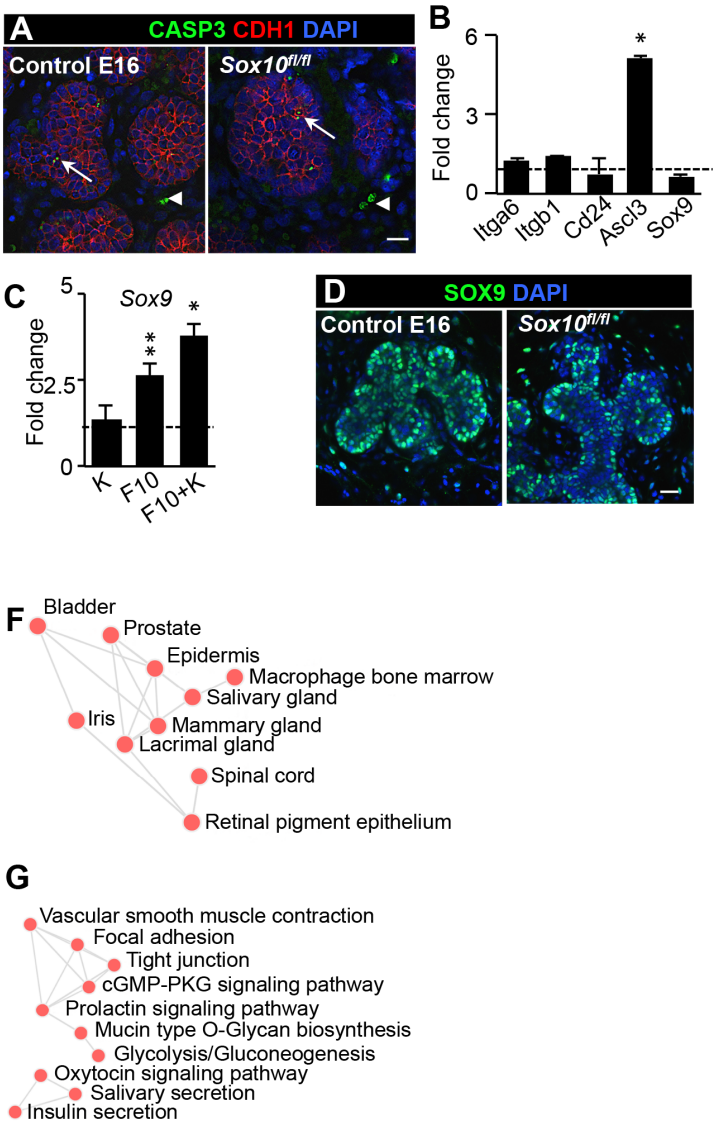

E

Gene	*- Log2* F.C.	*P*-value
Gyk	0.49	1.56E-05
Gm14584	0.49	7.96E-05
Cited4	0.49	1.54E-04
Lpo	0.49	1.62E-04
Abcc8	0.49	1.12E-04
Trpv6	0.48	5.30E-05
Tnfrsf11a	0.48	4.65E-05
Pgm5	0.48	3.55E-05
Cited1	0.48	2.17E-04
B3galt5	0.47	1.71E-06
Ceacam1	0.47	3.11E-05
Rap1gap	0.47	2.47E-04
Nrg2	0.47	1.99E-04
Gm23455	0.46	1.35E-05
Wwc1	0.46	5.03E-05
Nkx3-1	0.45	2.64E-04
Galnt7	0.45	7.37E-05
Bcar3	0.44	3.75E-05
Sntb1	0.44	6.01E-05
Ssfa2	0.43	3.02E-05
Gucy1b3	0.42	6.44E-06
Abtb2	0.40	9.90E-05
Btnl9	0.40	2.59E-04
Gm24357	0.39	2.63E-04
Dll1	0.37	1.88E-04
Esp8	0.37	2.19E-04
Msrb3	0.37	7.89E-05
Eno1	0.37	5.87E-05
Smyd5	0.36	1.73E-04
Papl	0.35	5.93E-05
Mylk	0.34	1.12E-05
Smr3a	0.32	7.41E-05
Synj2	0.30	1.73E-04
Ntn1	0.26	2.61E-04

SUPPLEMENTAL FIGURE 5

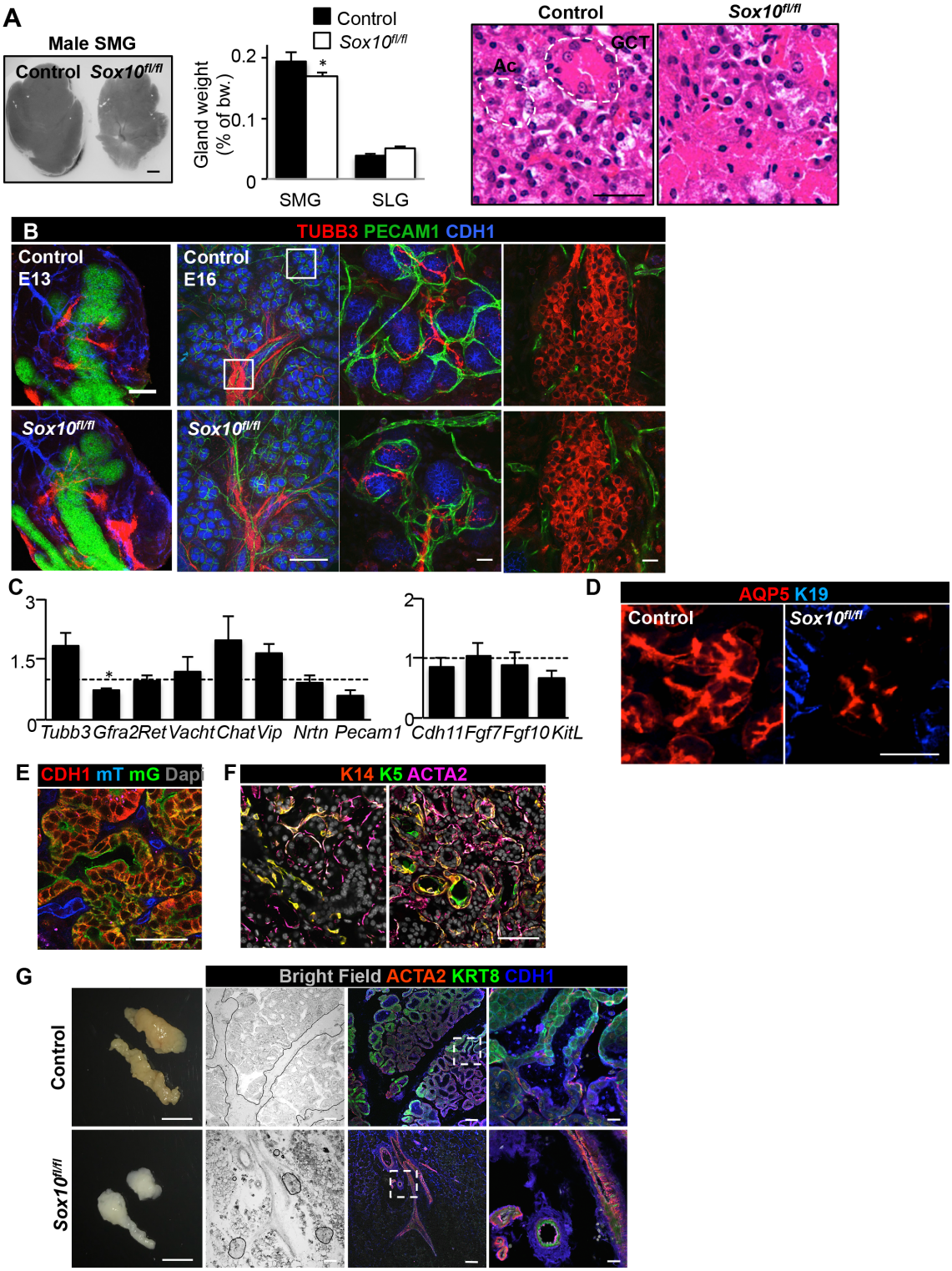

SUPPLEMENTAL FIGURE 6

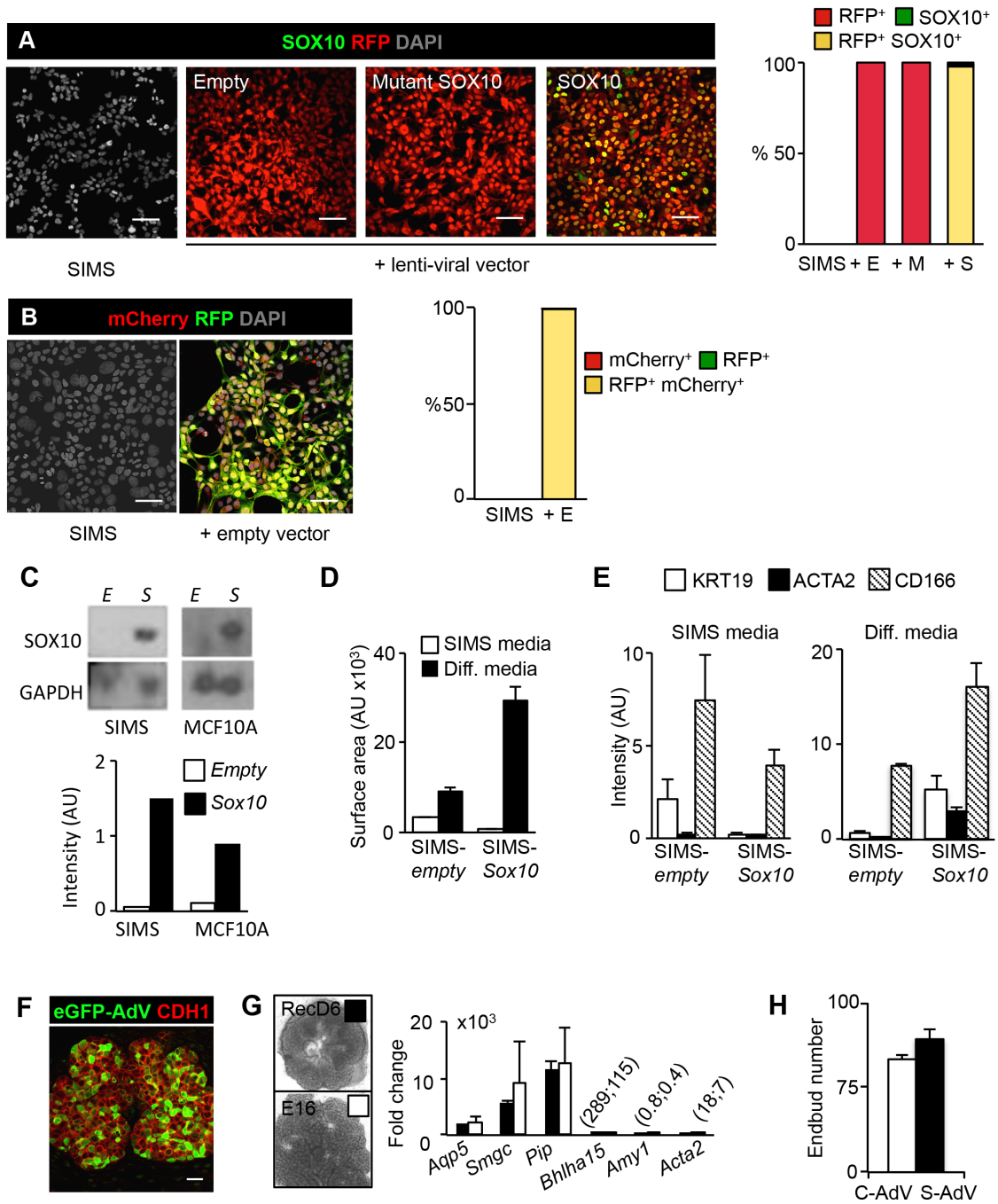

SUPPLEMENTAL FIGURE LEGENDS

FIGURE S1. Expression patterns of KIT and Keratins in epithelia of developing exocrine glands, Related to Figure 1.

(A) Confocal images (overlay and split images) of isolated epithelia (E11.5-13) stained for KIT and E-cadherin (CDH1). Arrows indicate oral epithelium (E11.5), main duct and endbuds (E13), and salivary submandibular gland (SMG, dotted arrow). Scale bar, 100 μm.

(B-C) Maximum projection and high power 2μm confocal image of isolated E12 SMG epithelia with attached oral epithelium stained for K14, K5, and K19. Dotted line indicates border of $K14^{+}K5^{+}K19^{+}$ and $K14^{+}$ cells. Scale bar, 100 μm and 20 μm.

(D) Confocal images of E11.5 isolated SMG epithelia stained for SOX10, SOX2, K5 and/or K14. Arrows show $K14^{+}K5^{+}$ cells co-expressing SOX2. Scale bar, 20 μm.

(E) *Fgf10*$^{-/-}$ E11.5 isolated oral epithelia, stained for CDH1, KIT, SOX10 or SOX2, and DAPI. Arrow indicates non-epithelial neuronal $SOX10^{+}$ cell. Scale bar, 20 μm.

(F) Fold change in gene expression of *Sox2*, *Sox10* and *DNp63* in isolated E13 epithelia (epi) stimulated with FGF10 (F10, 100ng/mL) for 2 hours. Data was normalized to *Rps29* and unstimulated epithelia (dotted line), Mean±SEM, N=3, Unpaired t-test. *, P<0.05.

FIGURE S2. Contribution of early *Sox2* or *Sox10* cells to exocrine glands, Related to Figure 2.

Multiple transgenic mice designed for lineage tracing were crossed with *Rosa26*-mTmG mice to acquire tissue for confocal images. Images show $mGFP^{+}$ cells (mG) as green and

mTomato^{+} cells (mT) as red, with the exception of (C) and (F) where mT is pseudo-colored in blue.

(A) Confocal imaging of E14 SMG and SLG from *Sox2*-Cre mice. Scale bar, 100 μm.

(B) *Sox2*-Cre^{TM} mice crossed with *Rosa26*-mTmG mice were induced at E12-13 and adult SMG and SLG were analyzed by confocal microscopy. Intra-glandular striated ducts (SD), and inter-glandular excretory (ED), Wharton's and Barthon's ducts (WD and BD) are shown. Arrows indicate mG^{+} cells. Scale bar, 20 μm.

(C) Confocal imaging of adult SMG sections from *Sox10*-Cre mice, co-stained for KRT8, ACTA2 or AQP5. Arrows represent mGFP^{+} cells co-expressing KRT8, ACTA2 or AQP5. Scale bar, 20 μm. Graph represents quantification (%) of all ACTA2^{+} and AQP5^{+} cells expressing mGFP. Mean±SEM, N>3 with scoring of more than 3 areas with 3 slides per SMG.

(D) Lineage tracing of *Sox10*-Cre mice at E14 (endbuds and main duct region) and adult SMGs were analyzed by confocal microscopy. Scale bar, 20 and 100 μm.

(E) Adult *Sox10*-Cre lacrimal (LG), parotid (PAR), sublingual glands (SLG) and designated main duct were analyzed by confocal microscopy. Scale bar, 20 and 100 μm.

(F) Adult SMG cryosections stained for K19, AQP5 and ACTA2 were analyzed by confocal microscopy. Glands derived from *Sox10*-rtTA;*Tet*-Cre mice were crossed with *Rosa26*-mTmG mice and induced with doxycycline from E9-12. Scale bar, 20 μm. Graph represents quantification of AQP5+ (84.7±0.1%), ACTA2+ (85.5±0.1%) and K19+ (90.9±0.1%) cells co-expressing mGFP or mTomato. N>3 with scoring of more than 3 areas with 3 slides per SMG.

FIGURE S3. Loss of *Sox10* impacts overall exocrine gland development, Related to Figure 3.

(A) Confocal pictures of KIT, SOX10 and KI67 co-staining in E13 and E16 SMG endbuds. Scale bar, 20 μm. Graph represents KIT^+ subpopulations counted on multiple sections through endbuds at each time-point. *N*>3, Mean ± SEM.

(B) Graphical outline demonstrating Cre-*flox* system used with the *Krt14* promoter, $Sox10^{flox/flox}$ and/or *Rosa26*-mTomato-mGFP (mTmG) mice.

(C) Confocal image of E16 control (*Rosa26*-mTmG) and $Sox10^{fl/fl}$ SMG endbuds, stained for SOX10. Scale bar, 20 μm.

(D) Quantification of endbud number in E16 SMGs from control and $Sox10^{fl/fl}$ mice. Data was normalized to control (C), Mean±SEM, *N*>3, Unpaired *t*-test. ****, *P*<0.0001. Control (100.0±6.3% endbuds); $Sox10^{fl/fl}$ (64.8±2.8% endbuds).

(E) Fluorescent image of mGFP expression in P1 SMG and SLG of $SOX10^{fl/+}$ control (*K14*-Cre*;Rosa26*-mTmG) and $Sox10^{fl/fl}$ mice. Scale bar, 500 μm.

(F) Fluorescent images of mGFP expression, pseudo-colored in black and white, of lacrimal gland and parotid gland of E16 control and $Sox10^{fl/fl}$ mice. Scale bar, 500 μm.

(G) Quantification of endbud number in E14 SLGs from control and $Sox10^{fl/fl}$ mice. Mean ± SEM, *N*>3, Unpaired *t*-test. *, *P*<0.05. Control (9.3±1.2) vs $Sox10^{fl/fl}$ (6.7±0.7).

Figure S4. Analysis of E16 $Sox10^{fl/fl}$ SMGs and changes in cell plasticity by forced overexpression of *Sox10*, Related to Figure 4.

(A) Confocal image representing distal area of E16 control or $Sox10^{fl/fl}$ SMGs. Tissue was stained for cleaved-caspase 3 (CASP3), E-cadherin (CDH1) and nuclei (DAPI). Arrows

indicate cell apoptosis in epithelia, arrowheads indicate cell death in surrounding environment. Scale bar, 20 μm.

(B) Fold changes in expression of progenitor-related markers in E16 *Sox10*$^{fl/fl}$ SMGs. Data was normalized to *Rps29* and control (dotted line). Mean±SEM, *N*>3, Multiple comparison *t*-test. *, *P*<0.05.

(C) Fold change in expression of *Sox9* in isolated E13 epithelia after a 3 hour stimulation with ligands KIT Ligand (K, 100ng/mL) and/or FGF10 (F10, 100ng/mL) to activate KIT/FGFR2b signaling. Data was normalized to *Rps29* and unstimulated epithelia (dotted line). Mean±SEM, *N*>3, Unpaired *t*-test. **, *P*<0.01; *, *P*<0.05.

(D) SMGs from E16 control and *Sox10*$^{fl/fl}$ mice were stained for SOX9 and DAPI, and analyzed by confocal microscopy. Scale bar, 20 μm.

(E) Continuing list of downregulated genes in E16 *Sox10*$^{fl/fl}$ SMGs versus control from Figure 4. The list was generated after bioinformatical analysis of next-generation sequencing data and cut-off at *Log2* fold change *(F.C)* of -0.25.

(F-G) Bioinformatic analysis of next-generation sequence performed on E16 control and *Sox10*$^{fl/fl}$ SMGs. Data was used as input for computing enrichment with existing lists of mouse gene atlas (F), and KEGG pathways (G).

Figure S5. Cellular changes in developing and adult *Sox10*$^{fl/fl}$ SMGs, Related to Figure 5.

(A) Bright field images of adult male SMGs from control and *Sox10*$^{fl/fl}$ mice. Scale bar, 1 mm. Graphs represent weight of SMGs as a percentage of body weight (bw.). Male SMG (control: 0.19±0.01%, *Sox10*$^{fl/fl}$: 0.16±0.01%). Male SLG (control: 0.03±0.01%, *Sox10*$^{fl/fl}$:

0.04±0.01%). Mean±SEM, *N*>3, Unpaired *t*-test. *, *P*<0.05. Hematoxylin-Eosin staining of SMGs of control and *Sox10*$^{fl/fl}$ mice. Scale bar, 25 μm. Acini (Ac) and granulated convoluted tubules (GCT), which are predominantly present in male glands, are outlined.

(B) Confocal imaging of E13 and E16 control and *Sox10*$^{fl/fl}$ SMGs, co-stained for TUBB3, PECAM1 and E-cadherin (CDH1). White boxes around the distal endbuds or ganglia are enlarged. Scale bar, 100 and 20 μm.

(C) qPCR analysis of environmental-related genes of E16 control and *Sox10*$^{fl/fl}$ SMGs. Data was normalized to *Rps29* and control (dotted line). Mean±SEM, *N*>3, Unpaired *t*-test. *, *P*<0.05.

(D) High power confocal image of AQP5 protein expression in epithelial cells from E16 control and *Sox10*$^{fl/fl}$ SMGs. Scale bar, 20 μm.

(E) Confocal image of adult SMG from the *Krt14*-Cre;*Sox10*$^{flox/flox}$*;Rosa26*-mTmG mouse. Tissue was co-stained for E-cadherin (CDH1). mTomato was pseudo-colored in blue. Scale bar, 20 μm.

(F) Outline of myoepithelial cells, expressing ACTA2, K14 and K5 in E16 control and *Sox10*$^{fl/fl}$ SMGs. Scale bar, 20 μm. Yellow represents overlap of K14 and K5 only in ducts.

(G) Bright field pictures of mammary glands (MMGs) from lactating control and *Krt14*-Cre;*Sox10*$^{flox/flox}$ mice. Scale bar, 0.5 cm (left). Staining of ACTA2, KRT8 and E-cadherin (CDH1) on MMG sections from control and *Krt14*-Cre;*Sox10*$^{flox/flox}$ mice. In control MMG, myoepithelial cells are ACTA2^{+}. Alveolar cells are KRT8^{-}CDH1^{+}. Ductal cells are KRT8^{+}CDH1^{+}. Right images are higher power from insets. Scale bar, 100 μm (low power) and 20 μm (high power).

Figure S6. Cellular changes in developing and adult *Sox10*$^{fl/fl}$ SMGs, Related to Figure 6.

(A) An adult duct cell line was non-transduced or transduced with empty lenti-viral vectors or with vectors containing mutant or wild-type *Sox10*. After transduction, cells were stained for DAPI, SOX10 and mCherry (RFP). Graph depicts quantification (%) of transduced cells expressing RFP and/or SOX10. Scale bar, 50 μm.

(B) Cells were non-transduced or transduced with empty lenti-viral vector, and stained for RFP (pseudo-colored in green) and DAPI. Graph shows quantification of the number of cells expressing mCherry and/or RFP. Scale bar, 50 μm.

(C) Western blot analysis for SOX10 and GAPDH on SIMS or MCF10A cells with *empty* lenti-viral vectors (*E*, *Empty*) or vectors containing *Sox10* (*S*, *Sox10*). Graph depicts semi-quantified analysis of SOX10 expression intensity in each cell type from representative blot. Data was normalized to GAPDH, and depicted in arbitrary units (AU).

(D) Quantification of surface area (arbitrary units) of organoids created by SIMS-*empty* or SIMS-*Sox10* cells by D7 in SIMS or differentiation media. Mean±SEM, $N>3$.

(E) Quantification of fluorescence intensity (arbitrary units) of KRT19, ACTA2, or CD166 expression on SIMS-*empty* or SIMS-*Sox10* cells in SIMS or differentiation media. Mean±SEM, $N=3$.

(F) Primary fetal E13 isolated epithelia was transfected with *eGFP*-AdV MOI 50, then recombined with mesenchyme and ganglia, and analyzed after 4 days for transfection efficiency. Tissue was stained for eGFP and E-cadherin (CDH1). Scale bar, 10 μm.

(G) Bright field picture of recombined SMG cultured for 6 days (rec D6) or E16 in vivo SMG. Both tissues were compared for gene expression related to myoepithelial, intercalated duct and acinar markers. Data was normalized to *Rps29*. Mean±SEM, $N>3$.

(H) Quantification of endbud number in recombined $Sox10^{fl/fl}$ SMGs transduced with *eGFP*-AdV (C-AdV) or *Sox10*-AdV (S-AdV). Mean±SEM, $N>3$.

SUPPLEMENTARY MATERIALS AND METHODS

Animal care and use

All mice used in the study were housed and bred in Specific Pathogen Free (SPF) rooms located in the AAALAC-accredited University of Michigan vivarium at the North Campus Research Center or at NIDCR at NIH. For timed-matings the morning of plug detection was considered day 0.5 post-coitum. Genotyping of mice was performed on tail biopsies by PCR and agarose gel electrophoresis using specific primers. *Krt14*-Cre mice, as used in (Lombaert et al., 2013), were crossed with Gt(Rosa)26Sor $^{tm4(ACTB-tdTomato,-EGFP)Luo}$ (Jackson Laboratory) and/or *Sox10*$^{flox/flox}$ mice that were obtained from Dr. M. Wegner (Finzsch et al., 2010). Multiple mice were gifted from various sources: *Fgf10*$^{-/-}$ from Dr. I. Nobuyuki (Kyoto University), *Sox2*-Cre from Dr. Y. Yamada (NIH), *Sox2*-Cre^{TM} from Dr. K. Hochedlinger (Harvard, MGH) and *Sox10*-rtTA (Dr. M. Wegner). Also mice were purchased: *Sox10*-Cre, *Tet*-Cre and timed-pregnant ICR female mice (Harlan, IN). Both female and male mice were evaluated at adult stages, which was considered 6 weeks old and beyond.

Ex vivo organ culture, recombination assays and adenovirus transduction

Adenovirus transduction was performed by transfecting isolated epithelia for one hour with *Sox10*-AdV (Vector Biolabs, AdV-272873) or eGFP-AdV (Vector Biolabs, 1060) before recombination. The transfection efficiency of the AdV in fetal E13 epithelia was found to be 74±8%.

Quantitative PCR

cDNA was generated from DNAse-free RNA, amplified and gene expression was normalized to house-keeping gene, *Rps29*. Experiments were run in technical triplicates with at a minimum of three biological samples.

Immunohistochemistry/fluorescence

Fluorescently labeled secondary antibodies and DAPI were used to visualize the proteins and nuclei, and Zeiss Confocal microscopy was used to analyze the images.

Adult tissue was fixed in 4% formaldehyde and processed for OCT cryosections. Tissue was labeled with primary and secondary antibodies and imaged, similar to embryonic tissue. Adult tissue was also fixed in 4% formaldehyde and processed for paraffin embedding. Paraffin sections were stained for hematoxylin-eosin staining and analyzed by bright field microscopy. More info on the antibodies used can be found in Supplementary Data.

Primary antibodies used: ACTA2 (Sigma, A2547), TUBB3 (RnD Systems, MAB1195), AQP5 (Alomone, AQP-005), KRT7 (Abcam, Ab9021), KRT8 (DSHB, Troma I), GFP (Abcam, Ab13970), SMGc (Antibody Online, ABIN1104377), BHLHA15 (Abcam, ab187978), SOX10 (Santa Cruz, sc-17342), KIT (RnD systems, MAB1195), CDH1 (Cell Signaling, 3195S), KRT5 (Covance PRB-160P), KRT14 (Covance, PRB-155P), KRT19 (DSHB, TROMA III), PECAM1 (BD Biosciences, 553708), SOX2 (Santa Cruz, sc-17320), CCDN1 (Abcam, ab16663), cleaved CASPASE3 (Cell Signaling, 9661), SOX9 (Chemicon, Ab5535), and CD166 (Santa Cruz, sc-74558).

ImageJ was used to quantify endbud number using bright field pictures, or GFP intensity in designated field using fluorescent images, or for quantification of co-expressed mGFP in acinar (AQP5), myoepithelial (ACTA2) and ductal cells (KRT19).

Western blot analysis and coomassie staining

Protein from saliva was resolved on Bis-Tris gels, stained for coomassie (10mg protein loaded per lane) or transferred to membranes, and probed with antibodies for MUC10 (ProSci, 42-311) or alpha-amylase (Sigma, A8273) (20mg protein loaded per lane). West Dura reagent was used for visualization. A more detailed western protocol is described in (Lombaert et al., 2013).

RNA-sequencing and bioinformatics analysis

For each RNA sample, cDNA libraries were made using the T
rueSeq RNA Sample Preparation kit (Illumina). 50bp single-ends were sequenced on the Illumina HiSeq 2500. Quality control was performed on the raw sequencing reads using FASTQC. Consequently, reads were mapped to the Mus musculus genome (Build mm9) with TopHat2 using Bowtie2. PCA analysis was used to outline the experimental groups, and bioinformatics analysis was performed to provide a Log2 fold in expressions.

Lentiviral overexpression in MCF10A and SIMS cells

A constitutively active lentiviral backbone, pLVX-EF1alpha-IRES-mCherry, was utilized for the overexpression in which we cloned mouse *Sox10* that shares 99% homology with the human *Sox10.* The empty vector or mutated inactive version of *Sox10* that was

truncated for first 150bps was used as control, which does not form SOX10 protein. Each cell type was transfected for control and *Sox10* virus in a 24 well plate. The MOI was 20.1. Cells were passaged to a 10 cm plate before flow sorting. Cells with empty or *Sox10* overexpressed vectors were sorted against mCherry to attain a homogeneous population. Cells were maintained in a T75 flask, and each passage was used for qPCR analysis.

Alternatively, a LentiX Tet-ON 3G (Takarabio) doxycycline inducible system was utilized to induce *Sox10* in SIMS cells. SIMS cells were first infected with virus particles carrying the Tet-ON 3G backbone with a neomycin selection cassette. A stable SIMS-Tet cell line, with MOI 60.35, was hereby generated. *Sox10* was inserted in a puromycin selectable pLVX-TRE3G backbone. Stable SIMS-Tet cells were infected with MOI 64.9, and selected with puromycin and neomycin for a stable inducible cell line. Control cell line, pLVX-Empty, was generated using virus carrying the pLVX-TRE3G backbone, which was infected with MOI 62.9 to SIMS-Tet cells. The cell lines were induced using 1μg/mL concentration of doxycycline for experimental purposes. Upon daily doxycycline activation, the Tet-ON-*Sox10* cells showed similar results to constitutive expression of the SIMS-*Sox10*-mCherry cells.

3D culture of SIMS cells

Ten thousand empty or SOX10-overexpressing single SIMS cells (in 25μL) were plated in 3D Matrigel GFR (BD Biosciences)/rat collagen type I (60/40), and allowed to solidify for 20 minutes at 37C. Cells were grown either in SIMS media (Laoide et al., 1996) or differentiation-inducing media. The latter consists of SIMS media with Glutamax (1x),

ITS (1x), N2 supplement (1x), EGF (20ng/mL), Fgf2 (20ng/mL), Dexamethasone (1uM), Triiodothyronine (2nM), Retinoic acid (0.1uM), Hydrocortisone (0.4ug/mL), Cholera toxin (8.5ng/mL), and Calcium (0.8mM). In some occasions, 1μg/mL doxycycline was added and media was replaced every 2 days. Outgrowth of cells was observed at day 7 (D7). The surface area of growth was calculated, and cell containing 3D gels were processed for protein staining. *N*=3 biological samples for each condition.
Surface area or fluorescence intensity was calculated in Image J and represented in arbitrary units.

Statistical Analysis and Data Availability

Statistical significance was determined by *p*-values of less than 0.05, with all experiments having at least 3 biological replicates. Unpaired *t*-test was used when comparing two groups. Determining significance of individual variables within a group of variables tested under different conditions, a multiple comparison *t*-test was used. Graphs show Mean±SEM for each group. $P<0.05$ was considered statistically significant.
RNASeq data is available on the Gene Expression Omnibus (GEO) website (GSE123341).

REFERENCES

Finzsch, M., Schreiner, S., Kichko, T., Reeh, P., Tamm, E.R., Bosl, M.R., Meijer, D., and Wegner, M. (2010). Sox10 is required for Schwann cell identity and progression beyond the immature Schwann cell stage. J Cell Biol *189*, 701-712.

Laoide, B.M., Courty, Y., Gastinne, I., Thibaut, C., Kellermann, O., and Rougeon, F. (1996). Immortalised mouse submandibular epithelial cell lines retain polarised structural and functional properties. J Cell Sci *109 (Pt 12)*, 2789-2800.

Lombaert, I.M., Abrams, S.R., Li, L., Eswarakumar, V.P., Sethi, A.J., Witt, R.L., and Hoffman, M.P. (2013). Combined KIT and FGFR2b signaling regulates epithelial progenitor expansion during organogenesis. Stem Cell Reports *1*, 604-619.